

University of Dundee

Inverse Reconstruction of Cell Proliferation Laws in Cancer Invasion Modelling

Alwuthaynani, Maher; Trucu, Dumitru

Published in:
Mathematics in Applied Sciences and Engineering

DOI:
[10.5206/mase/13865](https://doi.org/10.5206/mase/13865)

Publication date:
2021

Licence:
CC BY

Document Version
Publisher's PDF, also known as Version of record

[Link to publication in Discovery Research Portal](#)

Citation for published version (APA):
Alwuthaynani, M., & Trucu, D. (2021). Inverse Reconstruction of Cell Proliferation Laws in Cancer Invasion Modelling. *Mathematics in Applied Sciences and Engineering*. <https://doi.org/10.5206/mase/13865>

General rights

Copyright and moral rights for the publications made accessible in Discovery Research Portal are retained by the authors and/or other copyright owners and it is a condition of accessing publications that users recognise and abide by the legal requirements associated with these rights.

- Users may download and print one copy of any publication from Discovery Research Portal for the purpose of private study or research.
- You may not further distribute the material or use it for any profit-making activity or commercial gain.
- You may freely distribute the URL identifying the publication in the public portal.

Take down policy

If you believe that this document breaches copyright please contact us providing details, and we will remove access to the work immediately and investigate your claim.

INVERSE RECONSTRUCTION OF CELL PROLIFERATION LAWS IN CANCER INVASION MODELLING

MAHER ALWUTHAYNANI AND DUMITRU TRUCU

ABSTRACT. The process of local cancer cells invasion of the surrounding tissue is key for the overall tumour growth and spread within the human body, the past 3 decades witnessing intense mathematical modelling efforts in this regard. However, for a deep understanding of the cancer invasion process, these modelling studies require robust data assimilation approaches. While being of crucial importance in assimilating potential clinical data, the inverse problems approaches in cancer modelling are still in their early stages. In this regard, questions concerning the retrieval of the characteristics of tumour cells motility, cells mutations, and cells population proliferation remain widely open. This study deals with the identification and reconstruction of the usually unknown cancer cell proliferation law in cancer modelling from macroscopic tumour snapshot data collected at some later stage in the tumour evolution. Considering two basic tumour configurations, associated with the case of one cancer cells population and two cancer cells sub-populations that exercise their dynamics within the extracellular matrix, we combine Tikhonov regularization and gaussian mollification approaches with finite element and finite differences approximations to reconstruct the proliferation laws for each of these sub-populations from both exact and noisy measurements. Our inverse problem formulation is accompanied by numerical examples for the reconstruction of several proliferation laws used in cancer growth modelling.

1. INTRODUCTION

Initiated with mutations in individual normal cells and followed by rapid accumulation of early localized cancer cells mass via intense mitotic activity, the development of solid malignant tumours undergo several key stages in its evolution. These range from local pre-metastatic invasion, to tumour induced angiogenesis and metastatic spread towards remote locations within the human body giving rise to secondary tumours [59]. With its dynamics several spanning spatial and temporal scales, there are several hallmarks that a malignant tumour progression exhibits. Among these hallmarks, of key importance for the early pre-metastatic tumour development are the abnormal proliferation, secretion of proteolytic enzymes, and invasion of the surrounding tissue [22, 23].

Besides the cancer cells population, a malignant solid tumour contains an entire community of cells (such as immuno-inflammatory cells, stromal cells, fibroblasts) which together with the cancer cells exercise their coupled dynamics within the extracellular matrix (ECM) [59]. Indeed, while consisting of a mixture of major fibres (such as collagen and fibronectin) and small fibrils as well as soluble components (such as calcium ions Ca^{2+}), the ECM not only provides the scaffold for the tissue, but also represents the environment for the complex cancer dynamics enabled through cell-cell and cell-matrix interactions that are mediated through intense molecular signalling [25, 26, 27, 46, 45].

Received by the editors 20 April 2021; accepted 2 August 2021; published online 8 August 2021.

Key words and phrases. Cell Proliferation Law Identification; Inverse Problems; Tikhonov Regularization; Cancer Invasion.

Well-known for significant alterations and damage caused within the human body, the progression of solid tumours is characterized by sustained cancer cells proliferation, secretion of both growth factors and matrix degrading enzymes (MDEs), and intense migration within the surrounding tissue [59]. While exploring any space created through the degradation of the ECM by the MDEs, in their collective migration the cancer cells combine random motility with directional movement triggered by cell-adhesion processes [37, 41, 58, 60]. Notable here is the well documented process of “*durotaxis*” of the cancer cells (i.e., movement towards stiffer ECM regions [46, 45]). In particular we distinguish here the “*haptotactic*” motility by which cancer cells migrate against ECM gradients towards higher ECM density regions [36].

Directly involved in underpinning the processes of both local tumour invasion and metastasis, the cancer cell proliferation plays a central role within the overall cancer growth and spread [22, 23, 59]. Mediated by the internal circadian clock and its relation to cell cycle [9, 19], cancer cell proliferation takes advantage of favourable metabolic conditions [62] and contributes directly not only to the increase in tumour cell mass but also in its heterogeneity [1, 49]. Indeed, during the mitotic process, cells can divide not only in two identical daughter cells, but can also give rise to a new lineages of cells due to genetic mutations during the DNA replication [24, 54]. The emerging cancer cell population heterogeneity is a key characteristic for all tumours [34], having major implications in the response of malignant tumour to treatment. Notable here is for instance the situation met in glioma progression where the multiple sub-populations of glioma cells exhibit non-uniform reaction to most available treatment strategies [12, 21].

The past four decades or so have witnessed intense modelling efforts addressing the process of cancer growth and spread [2, 3, 5, 4, 7, 8, 10, 13, 18, 20, 39, 40, 57]. These proposed a range of local continuum spatio-temporal approaches to address the tissue-scale (macro-scale) tumour dynamics, exploring increasing levels of tumour complexity by gradually accounting for higher degree of biological information enabling spatial transport, namely: undirected random movement, haptotactic directed cancer cells migration, secretion of MDEs followed by degradation and remodelling of the ECM. More recent modelling approaches (including those based on the theory of mixtures [11, 44, 47]) explored all these spatio-temporal dynamics of tumour spread by considering increasingly complex aspects regarding heterotypic nature of tumour microenvironment and tumour heterogeneity, including considering the case of coupled dynamics of multiple sub-populations of cancer cells that arise as a result of mutations from the initial cancer cell population [6, 15]. However, while most of these models considered the underlining proliferation process to be of logistic-type [21, 32], with alternative Gompertz and von Bertalanffy laws for cell population growth also being proposed and explored [14, 31, 56], the precise form of the cancer cells proliferation law remains a big unknown in cancer modelling.

Given the central role that the proliferation process plays within the entire cancer dynamics, the retrieval of the unknown proliferation law from measured data is of key importance for the understanding of tumour progression. Mathematically, this proliferation law reconstruction can be regarded as a source identification problem for a coupled system of parabolic equations. However, despite significant progress made for source identification problems (mostly for single reaction-diffusion equations [16, 29, 42, 43] and more recently for systems [30]), to the authors knowledge this particular inverse problem associated with solution-dependent source identification within systems of reaction-diffusion-taxis equations (induced by random motility and haptotactic cancer cells movement) with nonlinear coupling both in the source and the haptotaxis terms is novel and has not been addressed so far by previous works.

In this paper we address the new inverse problem concerning the retrieval of the unknown proliferation law within tumour invasion modelling that considers both random and directed haptotactic movement the tumour cells population which degrades and remodels the surrounding ECM density. To that end, for the tumour cells population, we consider two cases, namely: (1) the case of one cancer cell population; and (2) the case of two cancer cells sub-populations consisting of a primary tumour cell subpopulation and a mutated secondary tumour cell subpopulation. Furthermore, we assume the knowledge of additional information in terms of both exact and noisy measurements of the tumour constituent density at a later time in the tumour evolution. Finally, we test our inversion approach on several proliferation laws that are usually used in cancer modelling.

2. A BASIC CANCER INVASION MODEL WITH A SINGLE TUMOUR CELLS POPULATION

We first consider a simple macro-scale cancer dynamics (similar to the one considered in [5] but ignoring the matrix degrading enzymes) where the growing malignant tumour consisting of a cancer cell population $c(x, t)$ mixed with an ECM density $v(x, t)$ is assumed here to develop its coupled dynamics on a two-dimensional compact tissue domain $\Omega \in \mathbb{R}^2$ over a time interval $[0, T]$, *i.e.*, $(x, t) \in \Omega \times [0, T]$. In the presence of an unknown cancer cell proliferation law $f(c, v)$, per unit time the cancer cells population is assumed to exercised a spatial transport driven by a combination of random movement and haptotactic bias against ECM gradients. At the same time, the tumour cells degrade the ECM density and remodels its spatial distribution. Therefore, mathematically, the basic cancer invasion model that we consider here is of the form

$$\frac{\partial c}{\partial t} = D_1 \Delta c - \eta_1 \nabla \cdot (c \nabla v) + \underbrace{f(c, v)}_{\text{unknown proliferation}} \quad (2.1a)$$

$$\frac{\partial v}{\partial t} = -\rho c v + \mu_v (K_c - c - v)^+ \quad (2.1b)$$

where $K_c > 0$ represents the tissue carrying capacity, and $(K_c - c - v)^+ := \max((K_c - c - v)^+, 0)$, $\rho > 0$ is the rate at which the ECM is degraded in the presence of cancer cells, and $\mu_v \geq 0$ is the ECM remodelling rate. While the general proliferation law $f(c, v)$ is considered here to be unknown and its identification will be our main focus in this work, most modelling papers assume this law to be of logistic or Gompertz type [21, 32, 53]. These widely used proliferation laws are of the following forms:

- Logistic proliferation:

$$\bar{f}(c, e) := \mu_c c (K_c - c - e), \quad (2.2)$$

- Gompertz proliferation:

$$\bar{f}(c, e) := \mu_c c \log \left(\frac{K_c}{c + e} \right), \quad (2.3)$$

where $\mu_c > 0$ is an intrinsic proliferation rate that is usually taken to be either constant or ECM dependent, and e is the tissue environment density (that include ECM density), and which unless otherwise specified, this is taken to be the ECM density, *i.e.*, $e := v$, as it is the case for instance in model (2.1).

Finally, the cancer invasion coupled dynamics expressed in (2.1a) and (2.1b) is started with the initial conditions

$$c(x, 0) := c_0(x) \quad \text{and} \quad v(x, 0) := v_0(x), \quad (2.4)$$

where $c_0(\cdot)$ and $v_0(\cdot)$ are positive functions representing initial densities of cancer cells and ECM, respectively. Furthermore, as during the dynamics, the cells are not supposed to leave the tissue

region Ω , we assume here that the coupled dynamics (2.1a) and (2.1b) takes place in the presence of zero Neumann boundary conditions, namely:

$$\left. \frac{\partial c}{\partial n} \right|_{\partial\Omega} = 0 \quad \text{and} \quad \left. \frac{\partial v}{\partial n} \right|_{\partial\Omega} = 0, \quad (2.5)$$

where $n(\xi)$ is the usual normal direction at any given tissue boundary point $\xi \in \partial\Omega$. Finally, in the following sections, the tumour dynamics (2.1) together with the initial and boundary conditions and (2.4) and (2.5) will be referred to as the “*forward model*”.

3. INVERSE PROBLEM FOR THE UNKNOWN CANCER CELLS PROLIFERATION LAW IN MODEL (2.1)

Considering here the forward model defined by the tumour dynamics (2.1) in the presence of the initial and boundary conditions (2.4) and (2.5), we aim to reconstruct the unknown cancer cells proliferation law $f(c, v)$ from additional information enabled by measurements of the cancer cells and ECM densities taken at a later time $t_f > 0$ in the tumour evolution. These measurements are therefore given in the form of two functions on Ω that are considered to be known in advance, namely

$$c^*(\cdot) : \Omega \rightarrow \mathbb{R} \quad \text{for the cancer density,} \quad (3.1a)$$

$$v^*(\cdot) : \Omega \rightarrow \mathbb{R} \quad \text{for the ECM density.} \quad (3.1b)$$

In the following, we will explore the reconstruction of the unknown cancer cells proliferation law $f(c, v)$ when the known measurements $c^*(x)$ and $v^*(x)$ will be given both as exact (accurate) data and as noisy data, $\forall x \in \Omega$.

3.1. Inverse Problem Setup: Forward Solver Computational Formulation. Assuming a uniform discretization $\mathcal{G}_\Omega := \{(x_i, y_j)\}_{i,j=1\dots N}$ of step size $\Delta x = \Delta y > 0$ for a square maximal tissue region $\Omega \subset \mathbb{R}^2$ where the tumour exercise its dynamics, at any given time $t \in [0, t_f]$ the discretizations of cancer densities $c(\cdot, t)$ and $v(\cdot, t)$ are therefore given by the $N \times N$ matrices $\tilde{c}(t) := \{\tilde{c}_{i,j}(t)\}_{i,j=1\dots N}$ and $\tilde{v}(t) := \{\tilde{v}_{i,j}(t)\}_{i,j=1\dots N}$, with $\tilde{c}_{i,j}(t) := c((x_i, y_j), t)$ and $\tilde{v}_{i,j}(t) := v((x_i, y_j), t)$, $\forall i, j = 1 \dots N$.

Using the *a priori* knowledge that the cumulated ECM and cancer densities could not exceed the tissue carrying capacity K_c , the unknown proliferation law can therefore be written-down in terms of an unknown (for the moment) function $S^{c^*, v^*} : [0, K_c] \times [0, K_c] \rightarrow [0, \infty)$. Moreover, this unknown function S^{c^*, v^*} will be appropriately identified within a suitable family of function \mathcal{S} such that the corresponding solution for the tumour model (2.1) will match the measurements given in (3.1). Thus, denoting through $f^{c^*, v^*}(\cdot, \cdot)$ the unknown proliferation for which the corresponding solution of model (2.1) matches measurement (3.1), at each (x_i, y_j) we can write this as

$$f^{c^*, v^*}(\tilde{c}_{i,j}(t), \tilde{v}_{i,j}(t)) := \mathcal{F}_{i,j}(\tilde{c}(t), \tilde{v}(t), S^{c^*, v^*}),$$

where $\mathcal{F}(\cdot, \cdot, \cdot) := \{\mathcal{F}_{i,j}(\cdot, \cdot, \cdot)\}_{i,j=1\dots N}$, $\mathcal{F}(\cdot, \cdot, \cdot) : \mathbb{R}^{N \times N} \times \mathbb{R}^{N \times N} \times \mathcal{S} \rightarrow \mathbb{R}^{N \times N}$, represents a “*trial proliferation operator*”, which will be specified below alongside the family of functions \mathcal{S} . Indeed, assuming an uniform discretization for the domain $[0, K_c] \times [0, K_c]$ given by an equally spaced grid $\mathcal{G}_M := \{(\eta_l, \zeta_k)\}_{l,k=1\dots M}$ of step size $\Delta\eta = \Delta\zeta > 0$, the unknown function S^{c^*, v^*} will be identified through a suitable approximation within the following $M \times M$ -dimensional space of functions associated with \mathcal{G}_M , namely

$$\mathcal{S} := \left\{ s : [0, K_c] \times [0, K_c] \rightarrow \mathbb{R} \mid s|_{E_{l,k}} = \sum_{p,q=0,1} s(\eta_{l+p}, \zeta_{k+q}) \phi_{l+p,k+q}, \quad \forall E_{l,k} \in \mathcal{G}_M^{tiles} \right\} \quad (3.2)$$

where $\mathcal{G}_M^{tiles} := \{E_{l,k} := [\eta_l, \eta_{l+1}] \times [\zeta_k, \zeta_{k+1}] \mid l, k = 1 \dots M-1\}$, and $\forall E_{l,k} \in \mathcal{G}_M^{tiles}$, $\{\phi_{l+p,k+q}\}_{p,q=0,1}$ are the usual bilinear shape functions on $E_{l,k}$. Thus, for any candidate function $s \in \mathcal{S}$, the corresponding

trial proliferation operator \mathcal{F} has each of its components $\mathcal{F}_{i,j}, \forall i, j = 1 \dots N$, given by

$$\mathcal{F}_{i,j}(\tilde{c}^s(t), \tilde{e}^s(t), s) := \sum_{p,q=0,1} s(\eta_{l+p}, \zeta_{k+q}) \phi_{l+p,k+q}(\tilde{c}_{i,j}^s(t), \tilde{e}_{i,j}^s(t)), \quad (3.3)$$

with (l, k) being independent of its choice within the associated set of indices $\Lambda_{i,j}$, namely:

$$\Lambda_{i,j} := \{(l', k') \in \{1, \dots, M-1\} \times \{1, \dots, M-1\} \mid \exists E_{l',k'} \in \mathcal{G}_M^{tiles} \text{ such that } (\tilde{c}_{i,j}^s(t), \tilde{e}_{i,j}^s(t)) \in E_{l',k'}\}.$$

where $\tilde{c}^s(t)$ represents the proliferating cell population, and $\tilde{e}^s(t)$ represents the tissue environment. In particular, here the proliferating cells population $\tilde{c}^s(t) := \{\tilde{c}_{i,j}^s(t)\}_{i,j=1\dots N}$ and the tissue environment $\tilde{e}^s(t) = \tilde{v}^s(t) := \{\tilde{v}_{i,j}^s(t)\}_{i,j=1\dots N}$ represent the solutions at the grid points and time $t > 0$ for the cancer cells and ECM densities obtained with model (2.1) when this uses $\mathcal{F}_{i,j}(\tilde{c}^s(t), \tilde{v}^s(t), s)$ as proliferation law given in (3.3). Thus, model (2.1) can be recasted in space-discretized form as

$$\frac{\partial}{\partial t} \begin{bmatrix} \tilde{c}^s \\ \tilde{v}^s \end{bmatrix} = \begin{bmatrix} \mathcal{H}^1(\tilde{c}^s, \tilde{v}^s, s) \\ \mathcal{H}^2(\tilde{c}^s, \tilde{v}^s, s) \end{bmatrix}. \quad (3.4)$$

Here, $\mathcal{H}^1(\cdot, \cdot, \cdot) = \{\mathcal{H}_{i,j}^1(\cdot, \cdot, \cdot)\}_{i,j=1\dots N}$ represents the spatial discretization corresponding to the first equation in (2.1), and each of its components $\mathcal{H}_{i,j}^1(\cdot, \cdot, \cdot), \forall i, j = 1 \dots N$, are given by

$$\begin{aligned} \mathcal{H}_{i,j}^1(\tilde{c}^s(t), \tilde{v}^s(t), s) := & \frac{D_1}{(\Delta x)^2} (\tilde{c}_{i-1,j}^s(t) + \tilde{c}_{i+1,j}^s(t) + \tilde{c}_{i,j-1}^s(t) + \tilde{c}_{i,j+1}^s(t) - 4\tilde{c}_{i,j}^s(t)) \\ & - \frac{\eta_1}{2(\Delta x)^2} ((\tilde{c}_{i,j}^s(t) + \tilde{c}_{i+1,j}^s(t)) (\tilde{v}_{i+1,j}^s(t) - \tilde{v}_{i,j}^s(t)) - (\tilde{c}_{i,j}^s(t) + \tilde{c}_{i-1,j}^s(t)) (\tilde{v}_{i,j}^s(t) - \tilde{v}_{i-1,j}^s(t)) \\ & + (\tilde{c}_{i,j}^s(t) + \tilde{c}_{i,j+1}^s(t)) (\tilde{v}_{i,j+1}^s(t) - \tilde{v}_{i,j}^s(t)) - (\tilde{c}_{i,j}^s(t) + \tilde{c}_{i,j-1}^s(t)) (\tilde{v}_{i,j}^s(t) - \tilde{v}_{i,j-1}^s(t))) \\ & + \mathcal{F}_{i,j}(\tilde{c}^s(t), \tilde{v}^s(t), s). \end{aligned} \quad (3.5)$$

On the other hand $\mathcal{H}^2(\cdot, \cdot) = \{\mathcal{H}_{i,j}^2(\cdot, \cdot)\}_{i,j=1\dots N}$ represents the discretization of the ECM equation corresponding to the second equation in (2.1), and each of its components $\mathcal{H}_{i,j}^2(\cdot, \cdot), \forall i, j = 1 \dots N$, are given by

$$\mathcal{H}_{i,j}^2(\tilde{c}^s(t), \tilde{v}^s(t)) := -\alpha \tilde{c}_{i,j}^s(t) \tilde{v}_{i,j}^s(t) + \mu_2(K_c - \tilde{c}_{i,j}^s(t) - \tilde{v}_{i,j}^s(t))^+. \quad (3.6)$$

Finally, considering a uniform time discretization $\{t_n\}_{n=0\dots L}$, with of time step $\Delta t := T/(L-1)$, for each $n \in \{1, \dots, L\}$, a simple Euler time marching step for system (3.4) can be formalized as usual via the associated operator $\tilde{K}_s : \mathbb{R}^{N \times N} \times \mathbb{R}^{N \times N} \rightarrow \mathbb{R}^{N \times N} \times \mathbb{R}^{N \times N}$ given by

$$\tilde{K}_s \left(\begin{bmatrix} \tilde{c}^{s,n} \\ \tilde{v}^{s,n} \end{bmatrix} \right) := \begin{bmatrix} \tilde{c}^{s,n} \\ \tilde{v}^{s,n} \end{bmatrix} + \Delta t \begin{bmatrix} \mathcal{H}^1(\tilde{c}^{s,n}, \tilde{v}^{s,n}, s) \\ \mathcal{H}^2(\tilde{c}^{s,n}, \tilde{v}^{s,n}) \end{bmatrix}, \quad (3.7)$$

where $\tilde{c}^{s,n} := \tilde{c}^s(t_n)$, and $\tilde{v}^{s,n} := \tilde{v}^s(t_n)$, while the right hand side operators are correspondingly given $\mathcal{H}^1(\tilde{c}^{s,n}, \tilde{v}^{s,n}, s) := \mathcal{H}^1(\tilde{c}^s(t_n), \tilde{v}^s(t_n), s)$ and $\mathcal{H}^2(\tilde{c}^{s,n}, \tilde{v}^{s,n}) := \mathcal{H}^2(\tilde{c}^s(t_n), \tilde{v}^s(t_n))$. This however, enables us to formulate the “forward operator” K between the family of function \mathcal{S} where we search for the appropriate cancer cells proliferation function S^{c^*,v^*} and the space where the discretized measurements (3.1) are recorded. Hence, the forward operator $K : \mathcal{S} \rightarrow \mathbb{R}^{N \times N} \times \mathbb{R}^{N \times N}$ is defined as

$$K(s) := \underbrace{\tilde{K}_s \circ \tilde{K}_s \circ \dots \circ \tilde{K}_s}_{L-1 \text{ times}} \left(\begin{bmatrix} \tilde{c}_0 \\ \tilde{v}_0 \end{bmatrix} \right) \quad (3.8)$$

where $\tilde{c}_0 := \{c_0(x_i, y_j)\}_{i,j=1,\dots,N}$ and $\tilde{v}_0 := \{v_0(x_i, y_j)\}_{i,j=1,\dots,N}$ are the discretized initial conditions (2.4) for the governing tumour forward model. Hence, for each $s \in \mathcal{S}$, the forward operator K gives the spatio-temporal progression of the initial condition $[\tilde{c}_0, \tilde{v}_0]^T$ under the invasion model (2.1), which

is obtained when the cell proliferation law at each instance of time t is given by the trial proliferation operator \mathcal{F} evaluated on the 3rd variable at s (i.e., the proliferation law is given by $\mathcal{F}(\tilde{c}^s(t), \tilde{v}^s(t), s)$).

3.2. The Inverse Problem Regularization Approach. As we can immediately observe, from (3.7) and (3.8) we have that our forward operator K is given as a finite composition of affine functions of the form

$$\mathcal{S} \ni s \mapsto \tilde{K}_s \in \ell^2(\ell^2(\mathcal{E} \times \mathcal{E}); \ell^2(\mathcal{E} \times \mathcal{E})), \quad (3.9)$$

with $\ell^2(\ell^2(\mathcal{E} \times \mathcal{E}); \ell^2(\mathcal{E} \times \mathcal{E}))$ being the usual finite-dimensional Bochner space of square integrable vector-value functions [61] with respect to the counting measure (see [48], p. 27) that are defined on $\ell^2(\mathcal{E} \times \mathcal{E})$ and take values in $\ell^2(\mathcal{E} \times \mathcal{E})$, where $\mathcal{E} := \{E_{i,j}\}_{i,j=1\dots N}$ represents the standard basis of elementary matrices associated with the grid \mathcal{G}_Ω . As a direct consequence, we immediately obtain that this is both continuous and compact, from where we obtain that K is also closed and sequentially bounded [61]. Therefore, we obtain that K satisfies the hypotheses assumed in [17] that ensure convergence for the nonlinear Tikhonov regularization strategy given by the functionals $\{J_\alpha\}_{\alpha>0}$, where for $\alpha > 0$, $J_\alpha : \mathcal{S} \rightarrow \mathbb{R}$ is defined by

$$J_\alpha(s) := \left\| K(s) - \begin{bmatrix} \tilde{c}^* \\ \tilde{v}^* \end{bmatrix} \right\|_2^2 + \alpha \|s\|_2^2, \quad \forall s \in \mathcal{S}. \quad (3.10)$$

This enables us to identify S^{c^*, v^*} as the limit as $\alpha \rightarrow 0$ of the points of minimum s^α of J_α . The two norms involved in (3.10) represent the usual Euclidean norms on the corresponding finite dimensional spaces. Indeed, while the first is the standard Euclidean norm on $\mathbb{R}^{N \times N} \times \mathbb{R}^{N \times N}$, the second is also the Euclidean norm induced on the $M \times M$ -dimensional space of functions \mathcal{S} via the standard isomorphism that can be established between \mathcal{S} and $\mathbb{R}^{M \times M}$ by which each $s \in \mathcal{S}$ is uniquely represented through its nodal values $\{s(\eta_l, \zeta_k)\}_{l,k=1\dots M}$ with respect to the bilinear basis functions $\{\bar{\phi}_{l,k}\}_{l,k=1\dots M}$ associated to \mathcal{G}_M [28], i.e.,

$$\text{since } s = \sum_{l,k=1\dots M} s(\eta_l, \zeta_k) \bar{\phi}_{l,k}, \text{ we therefore make the identification: } s \equiv \{s(\eta_l, \zeta_k)\}_{l,k=1\dots M}. \quad (3.11)$$

Finally, in (3.10), \tilde{c}^* and \tilde{v}^* represent the discretized measurements of the densities of cancer cells and ECM given in equations (3.1a)-(3.1b), i.e., $\tilde{c}^* := \{c^*(x_i, y_j)\}_{i,j=1,\dots,N}$ and $\tilde{v}^* := \{v^*(x_i, y_j)\}_{i,j=1,\dots,N}$.

Here we consider that the measurements data given in (3.12a)-(3.12b) are either exact or are corrupted by a certain level $\delta \geq 0$. Thus, maintaining for simplicity the measurement notation unchanged, these measurements data are given by

$$\tilde{c}^*(x) = \tilde{c}_{exact}^*(x) + \delta \gamma_c(x), \quad (3.12a)$$

$$\tilde{v}^*(x) = \tilde{v}_{exact}^*(x) + \delta \gamma_v(x), \quad (3.12b)$$

where, $\forall x \in \Omega$, we have that $\tilde{c}_{exact}^*(x)$ and $\tilde{v}_{exact}^*(x)$ are assumed to be the exact data, and $\gamma_c(x)$ and $\gamma_v(x)$ are signal-independent noise generated from a Gaussian normal distribution with mean zero and standard deviations σ_c and σ_v , respectively, given by

$$\sigma_c := \frac{1}{\lambda(\Omega)} \int_{\Omega} \tilde{c}_{exact}^*(x) dx, \quad (3.13a)$$

$$\sigma_v := \frac{1}{\lambda(\Omega)} \int_{\Omega} \tilde{v}_{exact}^*(x) dx, \quad (3.13b)$$

with $\lambda(\cdot)$ being the usual Lebesgue measure. In the numerical results below, we generate the random variables $\gamma_c(x)$ and $\gamma_v(x)$ via MATLAB function *normrnd* by taking $\{\gamma_c(x_i, y_j)\}_{i,j=1\dots N} := \text{normrnd}(0, \sigma_c, N \times N)$ and $\{\gamma_v(x_i, y_j)\}_{i,j=1\dots N} := \text{normrnd}(0, \sigma_v, N \times N)$.

3.3. Reconstruction of the logistic and Gompertz laws in cancer model (2.1). We explore now the inversion approach that we formulated so far in the context of forward model (2.1) by proceeding with the reconstruction of two of the most widely used cancer cells proliferation laws, namely: (1) logistic proliferation; and (2) Gompertz proliferation.

Initial Conditions. The initial conditions (2.4) that we consider in the computations for the forward model (2.1) are taken here to be of the form

$$c_0(x) := 0.5 \left(\exp \left(-\frac{\|x - (2, 2)\|_2^2}{0.03} \right) - \exp(-9.407) \right), \quad (3.14a)$$

$$v_0(x) := 0.5 + 0.3 \cdot \sin(4\pi \cdot \|x\|_2), \quad \forall x \in \Omega \quad (3.14b)$$

To identify the cancer cells proliferation law, we consider both exact and noisy measurement data (3.12) as additional information for the forward model (2.1) in the presence of initial conditions (3.14) and boundary conditions (2.5). Specifically, we consider that the exact data (namely $\tilde{c}_{exact}^*(x)$ and $\tilde{v}_{exact}^*(x)$) that appear in (3.12) are given by the solution \bar{c} and \bar{v} at the final time $t_f := T$ for the forward model (2.1), i.e.,

$$\tilde{c}_{exact}^*(x) := \bar{c}(x, t_f) \quad \text{and} \quad \tilde{v}_{exact}^*(x) := \bar{v}(x, t_f), \quad \forall x \in \Omega, \quad (3.15)$$

which is obtained when (2.1) uses a known proliferation law $f(c, v)$ that is specified as appropriate for each of the two cases, namely:

Case 1: for the reconstruction of the logistic cancer cell proliferation law, model (2.1) uses the logistic cell proliferation law $\bar{f}(c, v)$ given in (2.2), i.e., $f(c, v) := \bar{f}(c, v)$;

Case 2: for the reconstruction of the Gompertz cancer cell proliferation law, model (2.1) uses the Gompertz cell proliferation law $\bar{f}(c, v)$ given in (2.3), i.e., $f(c, v) := \bar{f}(c, v)$.

For each regularization parameter $\alpha > 0$ considered here, the minimisation process for J_α is initiated with $s_0 = \mathbb{I} \times 10^{-3}$, (where \mathbb{I} represents the $M \times M$ matrix of ones), and for the actual minimisation we employed here the nonlinear minimisation MATLAB function *lsqnonlin*. Finally, since there are no data to test the trial proliferating operators beyond the *maximal accessible region* \mathcal{A}_c defined by the minimum and maximum values of the solution, i.e.,

$$\begin{aligned} \mathcal{A}_c &:= [\bar{c}^{min}, \bar{c}^{max}] \times [\bar{v}^{min}, \bar{v}^{max}], \text{ with:} \\ \bar{c}^{min} &:= \min_{(x,t) \in \Omega \times [0,T]} c(x, t), & \bar{c}^{max} &:= \max_{(x,t) \in \Omega \times [0,T]} c(x, t), \\ \bar{v}^{min} &:= \min_{(x,t) \in \Omega \times [0,T]} v(x, t), & \bar{v}^{max} &:= \max_{(x,t) \in \Omega \times [0,T]} v(x, t), \end{aligned}$$

the reconstructions in this section will be attempted only for the restriction of the sought proliferation laws to \mathcal{A}_c . An acceptable numerical reconstruction of the proliferation law S^{c^*, v^*} , i.e.,

$$S^{c^*, v^*} := s^{\alpha^*}, \quad (3.16)$$

is obtained for the choice of the regularization parameter α^* , which throughout this work is selected based on a standard discrepancy principle argument [35].

Figure 1 shows the reconstruction of the logistic cancer cell proliferation law for cancer model (2.1) in the presence of the measurements given by (3.12) and (3.15) that are considered here both exact and affected by a level of noise $\delta \in \{1\%, 3\%\}$. For comparison, the first row of this figure shows the true logistic proliferation law restricted at the maximal accessible region \mathcal{A}_c where the reconstruction is

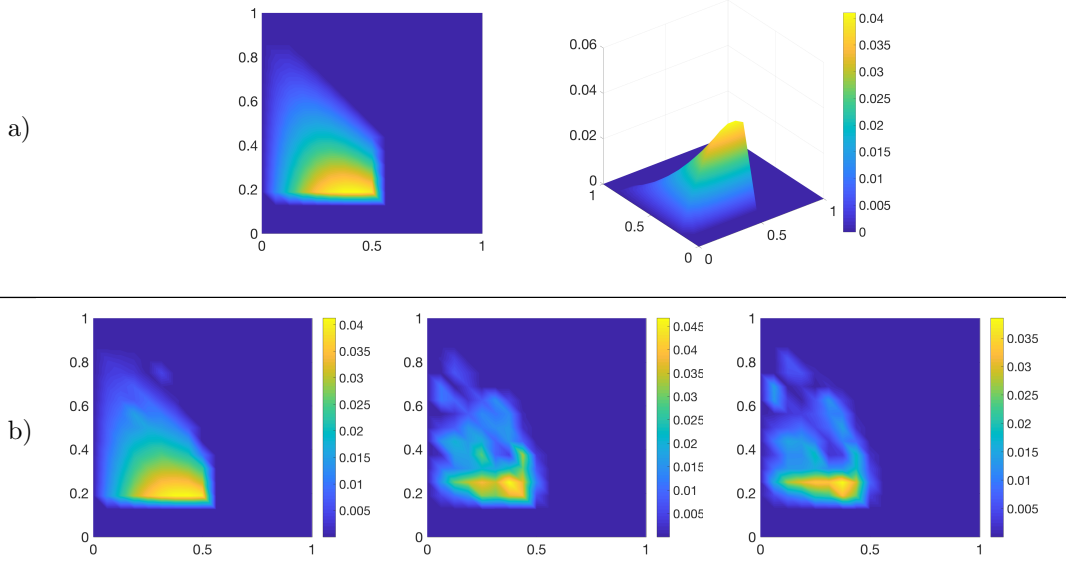


FIGURE 1. Reconstruction of logistic proliferation within model (2.1) obtained using the parameters given in Table 1: row a) the true logistic proliferation law restricted to \mathcal{A}_c ; row b) the reconstructed logistic proliferation law on \mathcal{A}_c in the presence of exact and noisy data. Row b) shows the reconstructions of logistic cancer cell proliferation law obtained for: (left) exact data and $\alpha^* = 10^{-10}$; (centre) 1% noisy data and $\alpha^* = 10^{-3}$; and (right) 3% noisy data and $\alpha^* = 10^{-2}$. For all plots in this figure we have that: 1) the first axis represents the the values for $c \in [\bar{c}^{min}, \bar{c}^{max}]$; 2) second axis represents the values for $v \in [\bar{v}^{min}, \bar{v}^{max}]$; and 3) the colour bars represent the magnitude of proliferation law or its reconstructions at each $(c, v) \in \mathcal{A}_c$.

being attempted. The second row of the figure show from left to right the reconstruction of the logistic proliferation law on \mathcal{A}_c with no noise, 1%, and 3% of noise in the measured data, respectively.

Similarly, Figure 2 shows the reconstruction of Gompertz cancer cell proliferation law for cancer model (2.1) in the presence of the measurements given by (3.12) and (3.15) that are considered here both exact and affected by a level of noise $\delta \in \{1\%, 3\%\}$. Again, the first row shows the true Gompertz law restricted to \mathcal{A}_c where the reconstruction is attempted. The second row of the figure show from left to right the Gompertz proliferation reconstruction on \mathcal{A}_c with no noise, 1%, and 3% of noise in the measured data, respectively.

From Figure 1 and Figure 2 we observe that we obtain good proliferation laws reconstructions in both cases (i.e., logistic and Gompertz, respectively) when the measurement data are not affected by noise. However, as expected, as soon as the level of noise increases in the measurements, the reconstruction gradually loses accuracy both in the case of logistic law (shown in Figure 1) and in the case of Gompertz law (shown in Figure 2).

4. EXTENDED TUMOUR INVASION MODEL WITH TWO CANCER CELLS SUBPOPULATIONS

We expand now our investigation to explore the reconstruction of the cancer cell proliferation laws in the context of an extended tumour invasion model that assumes not just one but two cancer cells subpopulations. Indeed, as the tumour evolve, cells from the initial primary tumour cell population undergo genetic mutations and give rise to a second mutated cancer cell population [24, 54] that is usually more aggressive [52], spreading faster and further in the human tissue than the first one. In this context, the simultaneous identification of the unknown proliferation law for both primary and mutated cancer cells subpopulations from measured data a later time during the tumour evolution remains of

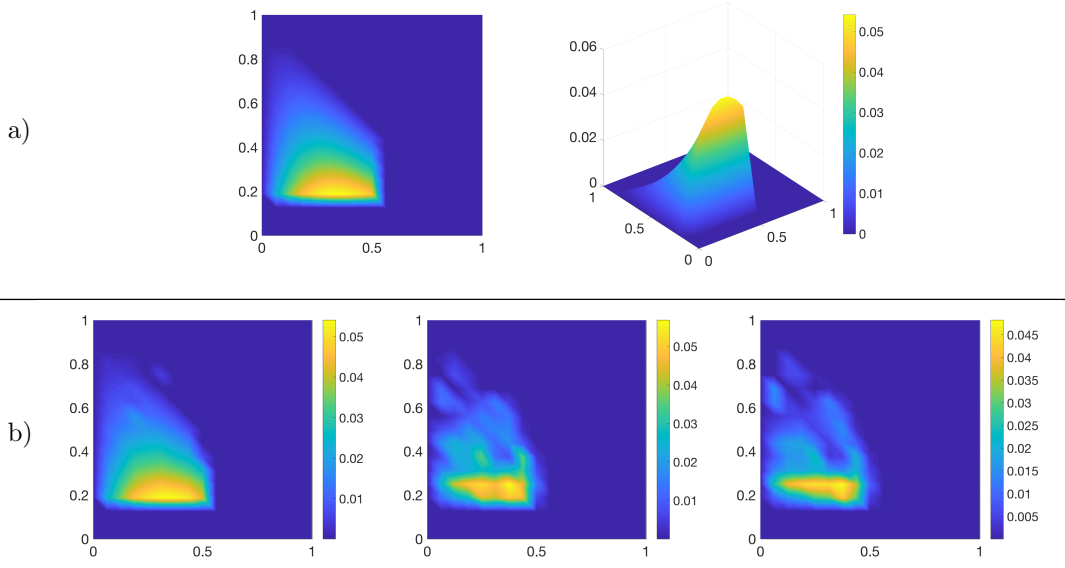


FIGURE 2. Reconstruction of Gompertz proliferation within model (2.1): row a) the true Gompertz proliferation law restricted to \mathcal{A}_c obtained using the parameters given in Table 1; row b) the reconstructed Gompertz proliferation law on \mathcal{A}_c in the presence of exact and noisy data. Row b) shows the reconstructions of Gompertz cancer cell proliferation law obtained for: (left) exact data and $\alpha^* = 10^{-8}$; (centre) 1% noisy data and $\alpha^* = 10^{-3}$; and (right) 3% noisy data and $\alpha^* = 10^{-3}$. For all plots in this figure we have that: 1) the first axis represents the values for $c \in [\bar{c}^{min}, \bar{c}^{max}]$; 2) second axis represents the values for $v \in [\bar{v}^{min}, \bar{v}^{max}]$; and 3) the colour bars represent the magnitude of proliferation law or its reconstructions at each $(c, v) \in \mathcal{A}_c$.

critical interest for the applicability of these models in concrete medical situations, where the estimate of the true extent of the tumour from available patient data is of paramount importance.

4.1. Two Cancer Cells Subpopulations Tumour Invasion Model. Denoting the density of the primary cancer cell subpopulation by $c_1(x, t)$ and the density of mutated cancer cells subpopulation by $c_2(x, t)$, these are mixed with a density of ECM (that continues to be denoted by $v(x, t)$) and together exercise a coupled spatio-temporal dynamics (on the tissue region Ω , over the time interval $[0, T]$) that is similar in nature to the one discussed in the case of a single cancer cell population captured by forward model (2.1). Indeed, while per unit time mutations occur between primary tumour cells and the mutated cancer cells, both subpopulations exercise a random movement and haptotactic directed motility on ECM gradients in the presence of a proliferation laws that here are considered unknown for each of the two subpopulations. On the other hand, both cancer cells degrade the ECM and contribute to its remodelling. Therefore, the tumour invasion coupled dynamics can be formalised mathematically

in this case as

$$\frac{\partial c_1}{\partial t} = D_1 \Delta c_1 - \eta_1 \nabla \cdot (c_1 \nabla v) + \underbrace{f_1(c_1, c_2, v)}_{\text{unknown proliferation}} - \underbrace{\mathcal{Q}(v, t) c_1}_{\text{mutation: } c_1 \rightarrow c_2}, \quad (4.1a)$$

$$\frac{\partial c_2}{\partial t} = D_2 \Delta c_2 - \eta_2 \nabla \cdot (c_2 \nabla v) + \underbrace{f_2(c_1, c_2, v)}_{\text{unknown proliferation}} + \mathcal{Q}(v, t) c_1, \quad (4.1b)$$

$$\frac{\partial v}{\partial t} = -\rho(c_1 + c_2)v + \mu_v (K_{cap}(\mathbf{c}, v) - v - c_1 - c_2), \quad (4.1c)$$

where D_p represents the diffusion coefficient while η_i is the haptotactic rate for population c_p , $p = 1, 2$. Further, as before, $\rho > 0$ is the ECM degradation rate, and $\mu_v \geq 0$ is the ECM remodelling rate. Finally, as the mutation rate from cancer cells subpopulation c_1 into subpopulation c_2 , $\mathcal{Q}(v, t)$, is dependent on both time and the ECM density levels [33], we adopt for this the modelling proposed [3, 15], and so mathematically we formalise this as

$$\mathcal{Q}(v, t) = \delta_m H(t - t_{1,2}) \cdot H(v(x, t) - v_{min}), \quad \forall (x, t) \in \Omega \times [0, t_f],$$

where $H(\cdot)$ denotes the usual Heaviside step function, $\delta_m > 0$ is the rate at which cellular mutations occur after a certain time $t_{1,2} > 0$ and in the presence of a minimal level of ECM $v_{min} > 0$.

Finally, the coupled dynamics (4.1a) - (4.1c) takes place in the presence of initial conditions

$$c_1(x, 0) := c_0(x), \quad c_2(x, 0) := 0, \quad \text{and} \quad v(x, 0) := v_0(x), \quad (4.2)$$

where $c_0(\cdot)$ and $v_0(\cdot)$ represent initial densities of primary cells subpopulation c_1 and ECM, respectively. Again, assuming as in the previous model that there is no cellular exchange or ECM flux across the tissue region boundaries, the coupled dynamics (4.1a) - (4.1c) is considered here in the presence of zero Neumann boundary conditions, namely:

$$\left. \frac{\partial c_1}{\partial n} \right|_{\partial \Omega} = 0, \quad \left. \frac{\partial c_2}{\partial n} \right|_{\partial \Omega} = 0 \quad \text{and} \quad \left. \frac{\partial v}{\partial n} \right|_{\partial \Omega} = 0. \quad (4.3)$$

4.2. Simultaneous Reconstruction of the Two Cancer Cells Proliferation Laws in Model (4.1). Building on the approach described in Section 3, we proceed now to address the simultaneous reconstruction of the unknown cancer cells proliferation laws $f_1(c_1, c_2, v)$ and $f_2(c_1, c_2, v)$ for primary and mutated cancer cell subpopulations from measured data

$$c_1^*(\cdot) : \Omega \rightarrow \mathbb{R} \quad \text{for the cancer subpopulation } c_1, \quad (4.4a)$$

$$c_2^*(\cdot) : \Omega \rightarrow \mathbb{R} \quad \text{for the cancer subpopulation } c_2, \quad (4.4b)$$

$$v^*(\cdot) : \Omega \rightarrow \mathbb{R} \quad \text{for the ECM density.} \quad (4.4c)$$

Furthermore, as we consider here both the case of exact and noisy data, we assume that the measured data (4.4) are of the same type as the ones considered in Section 3, and specifically these are given here as

$$\tilde{c}_p^*(x) = \tilde{c}_{p,exact}^*(x) + \delta \gamma_{c_p}(x), \quad p = 1, 2, \quad (4.5a)$$

$$\tilde{v}^*(x) = \tilde{v}_{exact}^*(x) + \delta \gamma_v(x), \quad (4.5b)$$

where, $\forall x \in \Omega$, we have that $\tilde{c}_{p,exact}^*(x)$, $p = 1, 2$, and $\tilde{v}_{exact}^*(x)$ are assumed to be exact data that may not be accessible in accurate form, and rather they would be affected by a level of noise $\delta \geq 0$. Further,

$\gamma_{c_p}(x)$, $p = 1, 2$, and $\gamma_v(x)$ are signal-independent noise which again are generated from a Gaussian normal distribution with mean zero and standard deviations

$$\sigma_{c_p} := \frac{1}{\lambda(\Omega)} \int_{\Omega} \tilde{c}_{p,exact}^*(x) dx, \quad p = 1, 2, \quad (4.6)$$

and σ_v (given in (3.13b)), respectively.

Using the setup already developed in Section 3, the unknown proliferation laws for both primary and mutated cancer cells subpopulations are expressed here again in terms of two unknown functions $S_p^{c_1^*, c_2^*, v^*} : [0, K_c] \times [0, K_c] \rightarrow [0, \infty)$ that correspond to each of the two tumour cell subpopulations c_p , $p = 1, 2$. This pair of functions $(S_1^{c_1^*, c_2^*, v^*}, S_2^{c_1^*, c_2^*, v^*})$ are going to be identified within the finite-dimensional space of functions $\mathcal{S} \times \mathcal{S}$ (with \mathcal{S} being the space defined in (3.2)) such that the measurements specified in (4.5a)-(4.5b) are matched by the solution at the final time t_f that is obtained for the two population cancer invasion model (4.1) for the resulting cell proliferation laws

$$f_p^{c_1^*, c_2^*, v^*}(c_{1,i,j}(t), c_{2,i,j}(t), v_{i,j}(t)) := \mathcal{F}_{i,j}(\tilde{c}(t), \tilde{e}_p(t), S_p^{c_1^*, c_2^*, v^*}) \quad \text{corresponding to } c_p, p = 1, 2. \quad (4.7)$$

Here, \mathcal{F} is the *trial proliferation operator* defined in (3.3) while $\tilde{e}_p(t)$ represent the tissue environments for each of the two cancer cells subpopulations c_p , $p = 1, 2$, and are given by $\tilde{e}_1(t) := \tilde{c}_2(t) + \tilde{v}(t)$ and $\tilde{e}_2(t) := \tilde{c}_1(t) + \tilde{v}(t)$.

Further, we note that, for any $\mathbf{s} := (s_1, s_2) \in \mathcal{S} \times \mathcal{S}$, an Euler time marching operator similar to \tilde{K}_s given in (3.7) can therefore be defined also in this case as

$$\tilde{\tilde{K}}_{\mathbf{s}} : \mathbb{R}^{N \times N} \times \mathbb{R}^{N \times N} \times \mathbb{R}^{N \times N} \rightarrow \mathbb{R}^{N \times N} \times \mathbb{R}^{N \times N} \times \mathbb{R}^{N \times N}$$

given by

$$\tilde{\tilde{K}}_{\mathbf{s}} \left(\begin{bmatrix} \tilde{c}_1^{\mathbf{s},n} \\ \tilde{c}_2^{\mathbf{s},n} \\ \tilde{v}^{\mathbf{s},n} \end{bmatrix} \right) := \begin{bmatrix} \tilde{c}_1^{\mathbf{s},n} \\ \tilde{c}_2^{\mathbf{s},n} \\ \tilde{v}^{\mathbf{s},n} \end{bmatrix} + \Delta t \begin{bmatrix} \mathcal{H}^1(\tilde{c}_1^{\mathbf{s},n}, \tilde{v}^{\mathbf{s},n}, s_1) - \mathcal{F}(\tilde{c}_1^{\mathbf{s},n}, \tilde{v}^{\mathbf{s},n}, s_1) + \mathcal{F}(\tilde{c}_1^{\mathbf{s},n}, \tilde{c}_1^{\mathbf{s},n}, s_1) - \mathcal{Q}(\tilde{v}^{\mathbf{s},n}, t_n) \\ \mathcal{H}^1(\tilde{c}_2^{\mathbf{s},n}, \tilde{v}^{\mathbf{s},n}, s_2) - \mathcal{F}(\tilde{c}_2^{\mathbf{s},n}, \tilde{v}^{\mathbf{s},n}, s_2) + \mathcal{F}(\tilde{c}_2^{\mathbf{s},n}, \tilde{c}_2^{\mathbf{s},n}, s_2) + \mathcal{Q}(\tilde{v}^{\mathbf{s},n}, t_n) \\ \mathcal{H}^2(\tilde{c}_1^{\mathbf{s},n} + \tilde{c}_2^{\mathbf{s},n}, \tilde{v}^{\mathbf{s},n}) \end{bmatrix}, \quad (4.8)$$

where $\tilde{c}_p^{\mathbf{s},n} := \tilde{c}_p^{\mathbf{s}}(t_n)$, and $\tilde{e}_p^{\mathbf{s},n} := \tilde{e}_p^{\mathbf{s}}(t_n)$, $p = 1, 2$. Moreover, in the right hand side, the operators \mathcal{H}^1 and \mathcal{H}^2 are the ones defined in (3.5)-(3.6), with

$$\mathcal{H}^1(\tilde{c}_p^{\mathbf{s},n}, \tilde{e}_p^{\mathbf{s},n}, s_p) := \mathcal{H}^1(\tilde{c}_p^{\mathbf{s}}(t_n), \tilde{e}_p^{\mathbf{s}}(t_n), s_p), p = 1, 2,$$

and

$$\mathcal{H}^2(\tilde{c}_1^{\mathbf{s},n} + \tilde{c}_2^{\mathbf{s},n}, \tilde{v}^{\mathbf{s},n}) := \mathcal{H}^2(\tilde{c}_1^{\mathbf{s}}(t_n) + \tilde{c}_2^{\mathbf{s}}(t_n), \tilde{v}^{\mathbf{s}}(t_n)).$$

Finally, \mathcal{F} is the *trial proliferation operator* given in (3.3), and

$$\mathcal{Q}(\tilde{v}^{\mathbf{s},n}, t_n) := \{\mathcal{Q}(v^{\mathbf{s}}((x_i, y_j), t_n), t_n)\}_{i,j=1 \dots N}$$

is the mutation term evaluated at the spatio-temporal grid nodes.

Finally, the family of operators $\{\tilde{\tilde{K}}_{\mathbf{s}}\}_{\mathbf{s} \in \mathcal{S} \times \mathcal{S}}$ enables us to obtain a similar “*forward operator*” to the one given in (3.8), which in this case is of the form

$$\overline{K} : \mathcal{S} \times \mathcal{S} \rightarrow \mathbb{R}^{N \times N} \times \mathbb{R}^{N \times N} \times \mathbb{R}^{N \times N}$$

given by

$$\overline{K}(\mathbf{s}) := \underbrace{\tilde{\tilde{K}}_{\mathbf{s}} \circ \tilde{\tilde{K}}_{\mathbf{s}} \circ \dots \circ \tilde{\tilde{K}}_{\mathbf{s}}}_{L-1 \text{ times}} \left(\begin{bmatrix} \tilde{c}_0 \\ \mathbf{0} \\ \tilde{v}_0 \end{bmatrix} \right), \quad \forall \mathbf{s} := (s_1, s_2) \in \mathcal{S} \times \mathcal{S}. \quad (4.9)$$

Thus, similar to Section 3.2, also in this case we obtain that the *forward operator* \bar{K} is given as a finite composition of affine functions of the form

$$\mathcal{S} \times \mathcal{S} \ni (s_1, s_2) =: \mathbf{s} \mapsto \tilde{\tilde{K}}_{\mathbf{s}} \in \ell^2(\ell^2(\mathcal{E} \times \mathcal{E} \times \mathcal{E}); \ell^2(\mathcal{E} \times \mathcal{E} \times \mathcal{E})) \quad (4.10)$$

with $\ell^2(\ell^2(\mathcal{E} \times \mathcal{E} \times \mathcal{E}); \ell^2(\mathcal{E} \times \mathcal{E} \times \mathcal{E}))$ being the usual finite-dimensional Bochner space of square integrable vector-value functions defined on $\ell^2(\mathcal{E} \times \mathcal{E} \times \mathcal{E})$ and taking values in the same space. From this, we obtain again that the mappings given in (4.10) are both continuous and compact, from where we obtain that \bar{K} is also closed sequentially bounded, and so the inverse problems hypotheses assumed in [17] are again satisfied. This ensures the convergence of the nonlinear Tikhonov regularization strategy defined by the functionals $\{\bar{J}_{\alpha_1, \alpha_2}\}_{\alpha_1, \alpha_2 > 0}$, where for $\alpha_1 > 0$ and $\alpha_2 > 0$, $\bar{J}_{\alpha_1, \alpha_2} : \mathcal{S} \times \mathcal{S} \rightarrow \mathbb{R}$ is defined by

$$\bar{J}_{\alpha_1, \alpha_2}(\mathbf{s}) := \left\| \bar{K}(s) - \begin{bmatrix} \tilde{c}_1^* \\ \tilde{c}_2^* \\ \tilde{v}^* \end{bmatrix} \right\|_2^2 + \alpha_1 \|s_1\|_2^2 + \alpha_2 \|s_2\|_2^2, \quad \forall \mathbf{s} := (s_1, s_2) \in \mathcal{S} \times \mathcal{S}. \quad (4.11)$$

This enables us to identify the pair of function $(S_1^{c_1^*, c_2^*, v^*}, S_2^{c_1^*, c_2^*, v^*})$ as the limit as $(\alpha_1, \alpha_2) \rightarrow (0, 0)$ of the points of minimum $\mathbf{s}^{\alpha_1, \alpha_2}$ of J_{α_1, α_2} . Here, \tilde{c}_1^* , \tilde{c}_2^* , and \tilde{v}^* represent the discretized measurements of the densities of cancer cells and ECM given in equations (3.1a)-(3.1b), i.e., $\tilde{c}_1^* := \{c_1^*(x_i, y_j)\}_{i,j=1,\dots,N}$, $\tilde{c}_2^* := \{c_2^*(x_i, y_j)\}_{i,j=1,\dots,N}$ and $\tilde{v}^* := \{v^*(x_i, y_j)\}_{i,j=1,\dots,N}$, respectively.

4.3. Reconstruction of the Logistic And Gompertz Laws in the Two Subpopulations Cancer Invasion Model (4.1). We explore now computationally the inversion approach that we formulated so far in the context of forward model for tumour invasion with two cancer cells subpopulations (4.1). To that end, we proceed with the simultaneous reconstruction of the proliferation laws for both cancer cell subpopulations in model (4.1) in two cases, namely: (1) logistic proliferation; and (2) Gompertz proliferation. Alongside the Neumann zero boundary conditions, model (4.1) assumes here the initial conditions (4.2), whose specific forms for the primary cell population and the ECM, namely c_0 and v_0 , being the ones given in (3.14a)-(3.14b)

To identify the cancer cells proliferation laws simultaneously for both cancer cell subpopulation, we consider both exact and noisy measurement data (3.1), for which, as in Section 3.2 the exact data (namely $\tilde{c}_{1,exact}^*(x)$, $\tilde{c}_{2,exact}^*(x)$ and $\tilde{v}_{exact}^*(x)$) that appear in (4.5) are given by the solution at the final time $t_f := T$ for the forward model (4.1), i.e.,

$$\tilde{c}_{1,exact}^*(x) := \bar{c}_1(x, t_f), \quad \tilde{c}_{2,exact}^*(x) := \bar{c}_2(x, t_f), \quad \text{and} \quad \tilde{v}_{exact}^*(x) := \bar{v}(x, t_f), \quad \forall x \in \Omega, \quad (4.12)$$

which is obtained when (4.1) uses known proliferation laws for primary and mutated cancer cell subpopulations. Specifically, these two known proliferation laws used in model (4.1) are of the form

$$f_1(c_1, c_2, v) := \bar{f}(c_1, c_2 + v) \quad \text{and} \quad f_2(c_1, c_2, v) := \bar{f}(c_2, c_1 + v), \quad (4.13)$$

being induced by a known law $\bar{f}(c, e)$ that is specified as appropriate in each of the following two cases, namely:

Case 1: for the reconstruction of the logistic cancer cell proliferation law, $\bar{f}(c, e)$ is the logistic law given in (2.2);

Case 2: for the reconstruction of the Gompertz cancer cell proliferation law, $\bar{f}(c, e)$ is the Gompertz law given in (2.3).

For each regularization parameter $\alpha > 0$ considered here, the minimisation process for J_{α_1, α_2} is initiated with $\mathbf{s}_0 := (s_{1,0}, s_{2,0})$, with $s_{1,0} = s_{2,0} = \mathbb{I} \times 10^{-3}$, (where \mathbb{I} represents the $M \times M$ matrix of ones). We explored the minimisation of J_{α_1, α_2} numerically for a range of regularization parameters

$\alpha_1, \alpha_2 \in \{10^{-i} \mid i = 1, \dots, 12\}$. Again, for the implementation of the minimisation of J_{α_1, α_2} we employed here the nonlinear minimisation MATLAB function *lsqnonlin*. Finally, since for each of the two cancer

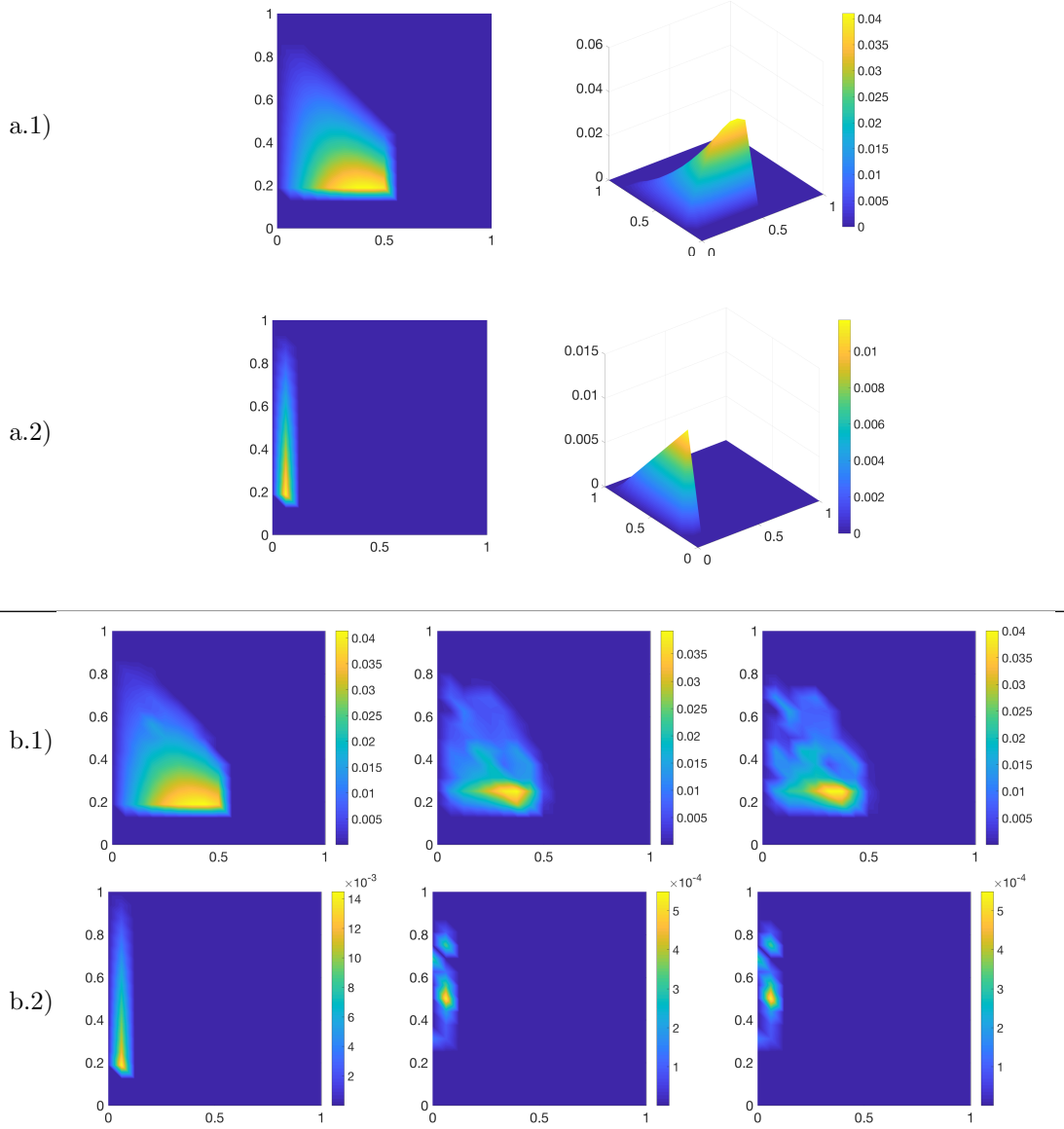


FIGURE 3. Reconstruction of logistic proliferation within model (4.1) obtained using the parameters given in Table 1. In rows a.1) and a.2) we have both p-color and graph plots of the true logistic proliferation laws for c_1 restricted to \mathcal{A}_{c_1} and c_2 restricted to \mathcal{A}_{c_2} , respectively. Row b.1) shows the reconstructions of logistic proliferation law obtained for c_1 on \mathcal{A}_{c_1} for: (left) exact data and $\alpha^* = 10^{-11}$; (centre) 1% noisy data and $\alpha^* = 10^{-3}$; and (right) 3% noisy data and $\alpha^* = 10^{-3}$. Row b.2) shows the reconstructions of logistic proliferation law obtained for c_2 on \mathcal{A}_{c_2} for: (left) exact data and $\alpha^* = 10^{-9}$; (centre) 1% noisy data and $\alpha^* = 10^{-3}$; and (right) 3% noisy data and $\alpha^* = 10^{-3}$. For all plots in this figure, for $i \in \{1, 2\}$ and $j \in \{1, 2\} \setminus \{i\}$, we have that: 1) the first axis represents the values for $c_i \in [\bar{c}_i^{min}, \bar{c}_i^{max}]$; 2) second axis represents the values for $c_j + v \in [\bar{c}_i^{min}, \bar{c}_i^{max}]$; and 3) the colour bars represent the magnitude of proliferation laws or their reconstructions at each $(c_i, c_j + v) \in \mathcal{A}_{c_i}$.

cell subpopulations c_i , $i = 1, 2$, there are no data to test the trial proliferating operators beyond the

maximal accessible regions \mathcal{A}_{c_i} defined by the minimum and maximum values of the solution, i.e.,

$$\begin{aligned} \mathcal{A}_{c_i} &:= [\bar{c}_i^{min}, \bar{c}_i^{max}] \times [\bar{e}_i^{min}, \bar{e}_i^{max}], \text{ with:} \\ \bar{c}_i^{min} &:= \min_{(x,t) \in \Omega \times [0,T]} c_i(x,t), & \bar{c}_i^{max} &:= \max_{(x,t) \in \Omega \times [0,T]} c_i(x,t), \\ \bar{e}_i^{min} &:= \min_{\substack{(x,t) \in \Omega \times [0,T] \\ j \in \{1,2\} \setminus \{i\}}} c_j(x,t) + v(x,t), & \bar{e}_i^{max} &:= \max_{\substack{(x,t) \in \Omega \times [0,T] \\ j \in \{1,2\} \setminus \{i\}}} c_j(x,t) + v(x,t), \end{aligned}$$

the reconstructions in this section will be attempted only for the restriction of the sought proliferation laws to \mathcal{A}_{c_i} .

Figure 3 shows the reconstruction of the logistic cancer cell proliferation laws for primary and mutated cancer cells subpopulations in model (4.1) in the presence of the measurements given by (4.5) and (4.12) that are considered here both exact and affected by a level of noise $\delta \in \{1\%, 3\%\}$. For comparison, in the upper half of this figure, rows a.1) and a.2) show the true logistic proliferation law restricted at the corresponding maximal accessible region \mathcal{A}_{c_1} and \mathcal{A}_{c_2} , respectively. In the bottom half of the figure, rows b.1) and b.2) shows reconstruction of the logistic proliferation laws for primary and mutated cancer cell subpopulations on \mathcal{A}_{c_1} and \mathcal{A}_{c_2} , respectively. From left to right in rows b.1) and b.2) we have the reconstruction of the logistic proliferation laws corresponding to each of the two cancer subpopulations from measurement data with no noise, 1%, and 3%, respectively.

Similarly, Figure 4 shows the reconstruction of the Gompertz cancer cell proliferation laws for primary and mutated cancer cells subpopulations in model (4.1) in the presence of the measurements given by (4.5) and (4.12). These measurements are considered here both as exact data and as data affected by a level of noise $\delta \in \{1\%, 3\%\}$. The figure respects the same structure as Figure 3, and so again, for comparison, in the upper half of this figure, rows a.1) and a.2) show the true Gompertz proliferation law restricted at the corresponding maximal accessible region \mathcal{A}_{c_1} and \mathcal{A}_{c_2} , respectively. In the bottom half of the figure, rows b.1) and b.2) shows reconstruction of the Gompertz proliferation laws for primary and mutated cancer cell subpopulations on \mathcal{A}_{c_1} and \mathcal{A}_{c_2} , respectively. From left to right in rows b.1) and b.2) we have the reconstruction of the two Gompertz proliferation laws corresponding to the two cancer subpopulations from measurement data with no noise, 1%, and 3%, respectively.

Figures 3 and 4 show that when the measurement data are not affected by noise we again obtain good reconstructions of the proliferation laws for both the primary and mutated cancer cells subpopulation in both in logistic and Gompertz case. However, as expected, as soon as the level of noise increases in the measurements, the reconstruction gradually loses accuracy both in the case of logistic law (shown in Figure 1) and in the case of Gompertz law (shown in Figure 2). Furthermore, we observe that, as the level of noise increases, the reconstruction of the mutated cancer cell population shown on rows b.2) of Figures 3 and 4 deteriorates faster than the reconstruction of the primary tumour cell population explored in the correspondingly noisy cases for both logistic and Gompertz laws and are shown in rows b.1) of Figures 3 and 4.

Finally, we also remark here that the primary tumour cells proliferations reconstructions for the two population model (4.1) in the noisy cases, shown in rows b.1) of Figures 3 and 4, deteriorates slightly faster (as the level of noise increases) than the cancer cells proliferation law reconstruction explored in the correspondingly noisy cases in the context of the one-population model (2.1) shown in rows b) of Figures 1 and 2.

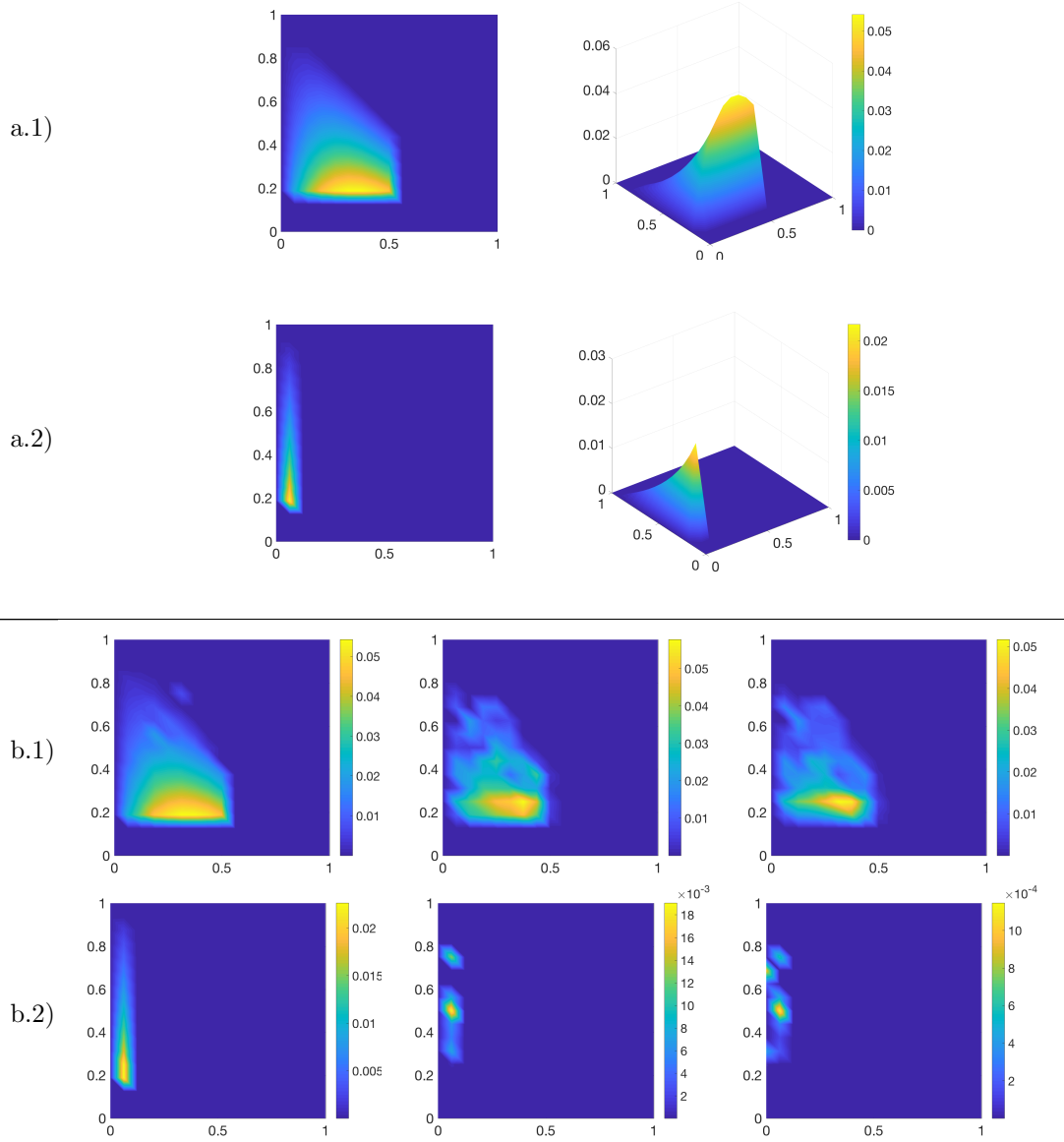


FIGURE 4. Reconstruction of Gompertz proliferation within model (4.1) obtained using the parameters given in Table 1. In rows a.1) and a.2) we have both p-color and graph plots of the true Gompertz proliferation laws for c_1 restricted to \mathcal{A}_{c_1} and c_2 restricted to \mathcal{A}_{c_2} , respectively. Row b.1) shows the reconstructions of Gompertz proliferation law obtained for c_1 on \mathcal{A}_{c_1} for: (left) exact data and $\alpha^* = 10^{-12}$; (centre) 1% noisy data and $\alpha^* = 10^{-3}$; and (right) 3% noisy data and $\alpha^* = 10^{-3}$. Row b.2) shows the reconstructions of Gompertz proliferation law obtained for c_2 on \mathcal{A}_{c_2} for: (left) exact data and $\alpha^* = 10^{-12}$; (centre) 1% noisy data and $\alpha^* = 10^{-4}$; and (right) 3% noisy data and $\alpha^* = 10^{-3}$. For all plots in this figure, for $i \in \{1, 2\}$ and $j \in \{1, 2\} \setminus \{i\}$, we have that: 1) the first axis represents the values for $c_i \in [\bar{c}_i^{min}, \bar{c}_i^{max}]$; 2) second axis represents the values for $c_j + v \in [\bar{c}_j^{min}, \bar{c}_j^{max}]$; and 3) the colour bars represent the magnitude of proliferation laws or their reconstructions at each $(c_i, c_j + v) \in \mathcal{A}_{c_i}$.

5. FURTHER REMARKS ON A SPECIAL CASE: THE RECONSTRUCTION THE BERTALANFFY LAW FOR THE TWO CANCER INVASION MODELS (2.1) AND (4.1)

Alongside logistic and Gompertz laws, another notable modelling approach for proliferation that was proposed in the cancer modelling literature is the von Bertalanffy law [14, 31, 56], which is of the form

$$\bar{f}(c, e) := \mu_c \left((K_c - e)^{1/3} c^{2/3} - c \right). \quad (5.1)$$

where, as in the case of (2.2)-(2.2), c stands for a generic cancer cell population density, and e represents the tissue environment density. However, the reconstruction of Bertalanffy proliferation law for cancer cells proliferation both for the case of one population model (2.1) and for the case of two population model (4.1) proves to be more challenging and requires further refinement of the approaches developed in Sections 3 and 4. Specifically, for a reasonable reconstruction of the Bertalanffy proliferation law requires the involvement of a mollified version of the trial proliferation operator \mathcal{F} given in (3.3) in each of the two modelling scenarios considered in this work, namely:

Case 1: cell proliferation reconstruction for the one cancer cell population tumour invasion model (2.1) with the measurement (3.12a)-(3.12b), where $\tilde{c}_{exact}^*(x)$ and $\tilde{v}_{exact}^*(x)$ are given by the solution at the final time of this model with zero-flux boundary conditions and initial conditions (3.14a)-(3.14b), i.e.,

$$\tilde{c}_{exact}^*(x) := \bar{c}(x, t_f) \quad \text{and} \quad \tilde{v}_{exact}^*(x) := \bar{v}(x, t_f), \quad \forall x \in \Omega, \quad (5.2)$$

which is obtained when the cell proliferation law is taken of the form $f(c, v) := \bar{f}(c, v)$, where $\bar{f}(\cdot, \cdot)$ is the law given in (5.1);

Case 2: cell proliferation reconstruction for the two cancer cells subpopulations tumour invasion model (4.1) with the measurements (4.5a)-(4.5b), where $\tilde{c}_{1,exact}^*(x)$, $\tilde{c}_{2,exact}^*(x)$, and $\tilde{v}_{exact}^*(x)$ are given by the solution at the final time of this with model zero-flux boundary conditions and the initial conditions for the primary subpopulation and ECM given in (3.14a)-(3.14b), i.e.,

$$\tilde{c}_{1,exact}^*(x) := \bar{c}_1(x, t_f), \quad \tilde{c}_{2,exact}^*(x) := \bar{c}_2(x, t_f), \quad \text{and} \quad \tilde{v}_{exact}^*(x) := \bar{v}(x, t_f), \quad \forall x \in \Omega, \quad (5.3)$$

which is obtained when the cell proliferation laws for each of the two cancer cell subpopulations are taken the form $f_1(c_1, c_2, v) := \bar{f}(c_1, c_2 + v)$ and $f_2(c_1, c_2, v) := \bar{f}(c_2, c_1 + v)$, where $\bar{f}(\cdot, \cdot)$ is again given the law in (5.1).

The *mollified trial proliferation operator* used here (instead of \mathcal{F}) is denoted by \mathcal{F}_ϵ , and is defined here as

$$\mathcal{F}_\epsilon(\cdot, \cdot, \cdot) : \mathcal{F}(\cdot, \cdot, \cdot) : \mathbb{R}^{N \times N} \times \mathbb{R}^{N \times N} \times \mathcal{S} \rightarrow \mathbb{R}^{N \times N}$$

given by

$$\mathcal{F}_\epsilon(\cdot, \cdot, \cdot) := \{\mathcal{F}_{i,j}(\cdot, \cdot, \cdot) * \psi_\epsilon\}_{i,j=1 \dots N}$$

where, $\forall i, j = 1 \dots N$, we have that $\mathcal{F}_{i,j}(\cdot, \cdot, \cdot)$ is the function defined in (3.3). Furthermore, the involved kernel ψ_ϵ is given by the standard mollifier of radius $\epsilon > 0$, namely

$$\psi_\epsilon(x) := \frac{1}{\epsilon^2} \psi\left(\frac{x}{\epsilon}\right)$$

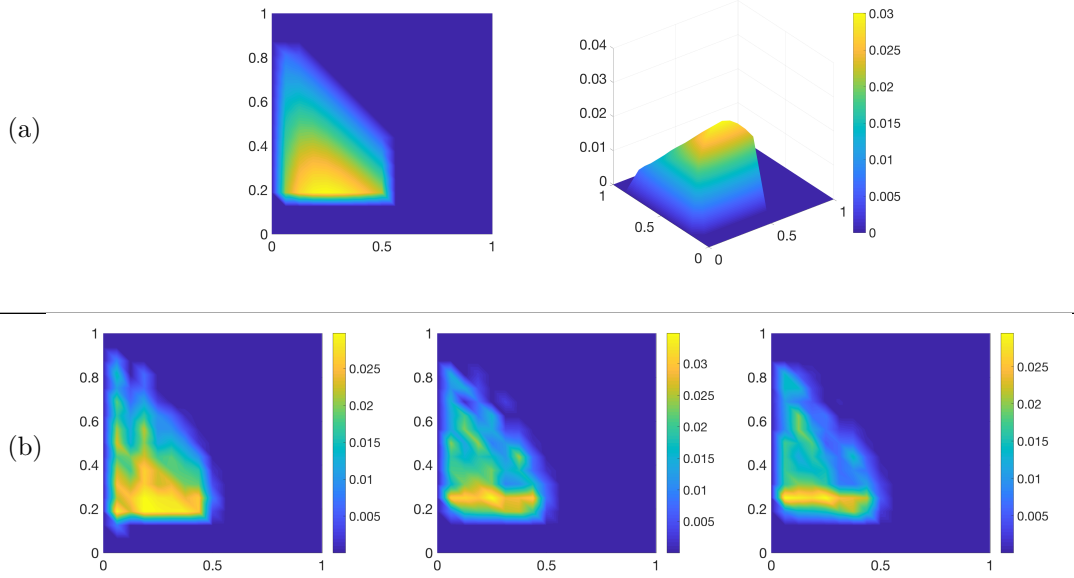


FIGURE 5. Reconstruction of von Bertalanffy proliferation within model (2.1) obtained using the parameters given in Table 1: row a) the true von Bertalanffy proliferation law restricted to \mathcal{A}_c ; row b) the reconstructed von Bertalanffy proliferation law on \mathcal{A}_c in the presence of exact and noisy data. Row b) shows the reconstructions of von Bertalanffy cancer cell proliferation law obtained for: (left) exact data and $\alpha^* = 10^{-3}$; (centre) 1% noisy data and $\alpha^* = 10^{-3}$; and (right) 3% noisy data and $\alpha^* = 10^{-3}$. For all plots in this figure we have that: 1) the first axis represents the values for $c \in [\bar{c}^{min}, \bar{c}^{max}]$; 2) second axis represents the values for $v \in [\bar{v}^{min}, \bar{v}^{max}]$; and 3) the colour bars represent the magnitude of proliferation law or its reconstructions at each $(c, v) \in \mathcal{A}_c$.

where ψ is the compact support function $\psi : \mathbb{R}^2 \rightarrow \mathbb{R}$ given by

$$\psi(x) := \begin{cases} \frac{\exp\left(\frac{-1}{1-\|x\|_2^2}\right)}{\int_{\mathbf{B}(0,1)} \exp\left(\frac{1}{1-\|z\|_2^2}\right) dz} & \text{if } x \in \mathbf{B}(0,1), \\ 0 & \text{if } x \notin \mathbf{B}(0,1), \end{cases}$$

with $\mathbf{B}(0,1)$ representing the open unit ball in \mathbb{R}^2 .

Figure 5 shows the reconstruction of the Bertalanffy cancer cell proliferation law for cancer model (2.1) in the presence of the measurements given by (3.12) and (5.2) that are considered here both exact and affected by a level of noise $\delta \in \{1\%, 3\%\}$. For comparison, again, row a) of this figure shows the true Bertalanffy proliferation law restricted at the maximal accessible region \mathcal{A}_c where the reconstruction is being attempted. Row b) of the figure shows from left to right the reconstruction of the Bertalanffy proliferation law on \mathcal{A}_c with no noise, 1%, and 3% of noise in the measured data, respectively.

Figure 6 shows the reconstruction of the Bertalanffy cancer cell proliferation laws for primary and mutated cancer cells subpopulations in model (4.1) in the presence of the measurements given by (4.5) and (5.2) that are considered here both as exact data and as data affected by a level of noise $\delta \in \{1\%, 3\%\}$. The figure respects the same structure as Figure 3 and 4, and so again, for comparison, in the upper half of this figure, rows a.1) and a.2) show the true Bertalanffy proliferation law restricted at the corresponding maximal accessible region \mathcal{A}_{c_1} and \mathcal{A}_{c_2} , respectively. In the bottom half of the figure, rows b.1) and b.2) show reconstruction of the Bertalanffy proliferation laws for primary and mutated cancer cell subpopulations on \mathcal{A}_{c_1} and \mathcal{A}_{c_2} , respectively. From left to right in rows b.1) and

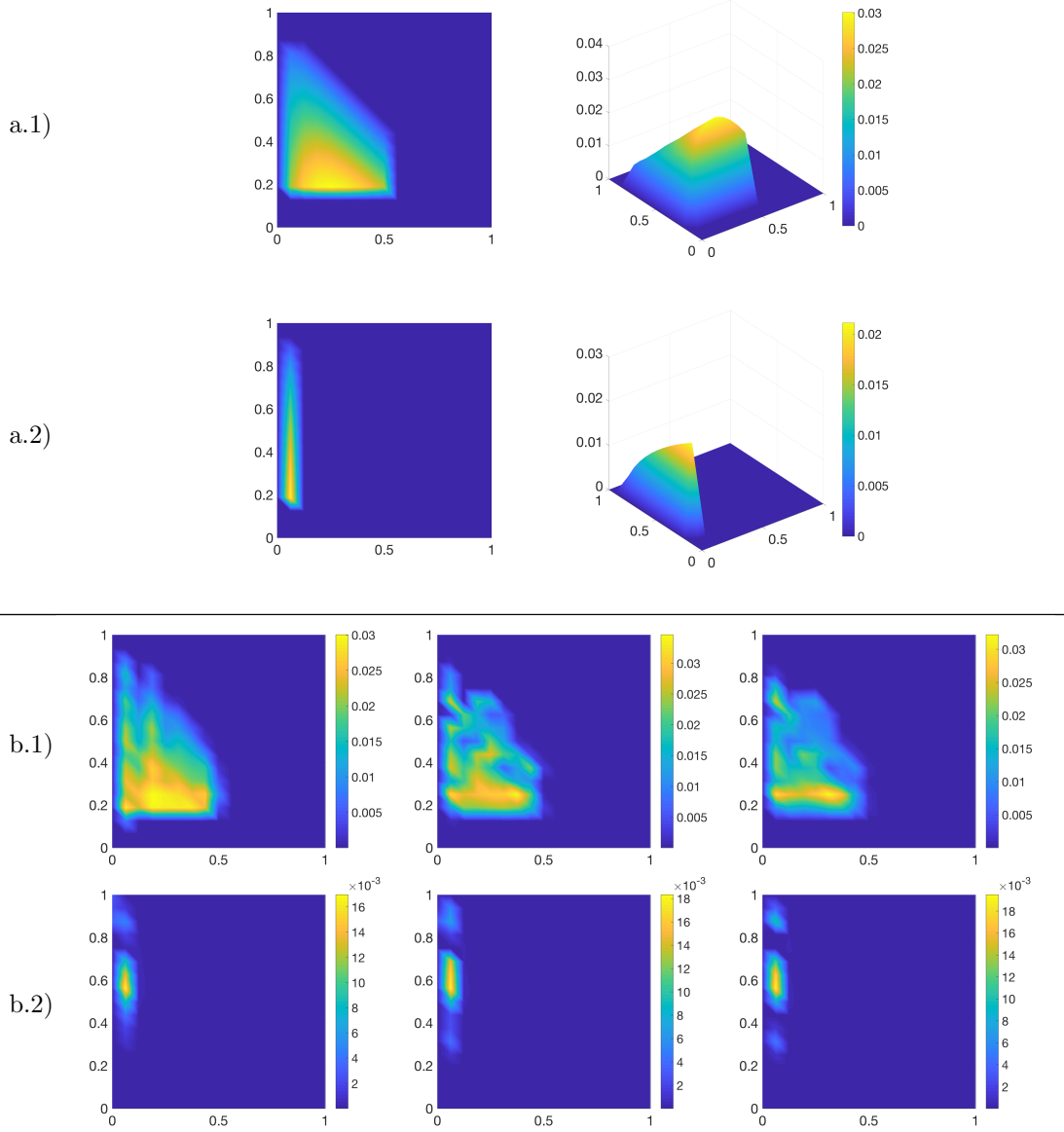


FIGURE 6. Reconstruction of Bertalanffy proliferation within model (4.1) obtained using the parameters given in Table 1. In rows a.1) and a.2) we have both p-color and graph plots of the true Bertalanffy proliferation laws for c_1 restricted to \mathcal{A}_{c_1} and c_2 restricted to \mathcal{A}_{c_2} , respectively. Row b.1) shows the reconstructions of Bertalanffy proliferation law obtained for c_1 on \mathcal{A}_{c_1} for: (left) exact data and $\alpha^* = 10^{-4}$; (centre) 1% noisy data and $\alpha^* = 10^{-3}$; and (right) 3% noisy data and $\alpha^* = 10^{-2}$. Row b.2) shows the reconstructions of Bertalanffy proliferation law obtained for c_2 on \mathcal{A}_{c_2} for: (left) exact data and $\alpha^* = 10^{-3}$; (centre) 1% noisy data and $\alpha^* = 10^{-3}$; and (right) 3% noisy data and $\alpha^* = 10^{-3}$. For all plots in this figure, for $i \in \{1, 2\}$ and $j \in \{1, 2\} \setminus \{i\}$, we have that: 1) the first axis represents the values for $c_i \in [\bar{c}_i^{min}, \bar{c}_i^{max}]$; 2) second axis represents the values for $c_j + v \in [\bar{c}_i^{min}, \bar{c}_i^{max}]$; and 3) the colour bars represent the magnitude of proliferation laws or their reconstructions at each $(c_i, c_j + v) \in \mathcal{A}_{c_i}$.

b.2) we have the reconstruction of the two Bertalanffy proliferation laws corresponding to the two cancer subpopulations from measurement data with no noise, 1%, and 3%, respectively.

6. CONCLUSION

In this work we explored a new inverse problem that addresses the reconstruction of the cancer cells proliferation law in cancer invasion modelling from available additional measurements taken in form of a spatial tumour snapshot data (which in practice can be provided through a medical imaging scan) that is acquired at a later stage in the tumour evolution. The investigation considers the cancer cells proliferation law reconstruction in the context of two tumour invasion models, namely: (1) for the case of single cancer cell population model (2.1); and (2) for the case of a model with two cancer cells subpopulations (4.1) where an initial primary tumour cells population mutates over time into a secondary tumour cells population whose proliferation law is also unknown and needs to be determined. For both modelling cases, we developed an inverse problem Tikhonov regularization-based approach, where the reconstruction of the proliferation law for the single cancer cell population in the case of model (2.1) as well as simultaneous reconstruction of the proliferation laws each of the two cancer cells subpopulations in model (4.1) is identified from additional information provided in the form of both exact and noisy measurements tumour.

This inverse problem approach is implemented computationally via a mixed finite differences - finite element numerical scheme. Specifically, on one hand, we use a Crank-Nicholson type finite difference scheme for the discretization of the involved *forward model* that arises in each of the two tumour invasion dynamics that we considered here (i.e., corresponding to an invading tumour with: (1) a single cancer cells population, and (2) two cancer cells subpopulations). On the other hand, we develop a finite element approach involving a bilinear shape functions on a square mesh for the discretization of proliferation laws candidates recruited from a proposed space of functions \mathcal{S} as well as their evaluation on a maximal accessible regions where the proliferation law reconstruction is performed. Finally, these two parts are appropriately assembled in an optimisation solver that seeks to reconstruct the cancer cell proliferation law by minimising the emerging Tikhonov functionals that are formulated in each of the two cases considered.

Finally, this inversion approach was explored and tested on the reconstruction cancer cell proliferation laws that are used in cancer modelling, namely: (i) logistic, (ii) Gompertz, and (iii) von Bertalanffy. While for exact measurement we obtain a good reconstruction both logistic and Gompertz laws, for increasingly noisy measurements the reconstruction gradually deteriorates. This degradation of the reconstruction in increasing noise regime is expected, this being more pronounced in for the identification of the mutated cell proliferation law within the cancer cells subpopulations (4.1), where the deterioration of the reconstruction is faster than that addressing the proliferation law for the primary tumour cell population. Finally, as the reconstruction of the von Bertalanffy law proved to be more challenging numerically both in the case of exact and measure data, for an acceptable reconstruction we amended our approach with a mollification approach for the *trial proliferation operator* that is involved in the formulation of the associated forward operator.

Future work will attempt the reconstruction of the proliferation laws when a more complex cell directed movement is considered, which besides haptotactic cell motility will include also the presence of chemotaxis (triggerred for instance by an incoming field of nutrients). Furthermore, this future investigation will also include an analytically and computational assessment of the influence the choice of the considered final-time measurements have over the reconstruction of the proliferation law.

ACKNOWLEDGEMENT

The first author would like to thank Saudi Arabian Cultural Bureau in the United Kingdom (UK-SACB) on behalf of Taif University and the University College of Al-Khurmah in Saudi Arabia for supporting and sponsoring his PhD studies at the University of Dundee.

APPENDIX A. PARAMETERS USED IN COMPUTATIONS

For all the cancer cells proliferation laws reconstructions considered in this work, we use the parameter set specified in Table 1.

Parameter	Value	Description	Reference
D_1	0.00675	diffusion of primary tumour	[15]
D_2	0.00675	diffusion of secondary tumour	[15]
η_1	2.85×10^{-2}	haptotaxis to ECM from c_1	[38]
η_2	2.85×10^{-2}	haptotaxis to ECM from c_2	[38]
μ_c	0.25	proliferation of tumour cells c	[50]
K_c	1	tissue carrying capacity	[55]
ρ	2	ECM degradation coefficient	[51]
μ_v	0.40	ECM remodelling coefficient	[55]
$t_{1,2}$	10	time initiation for mutations	[50, 3]
δ_m	0.3	mutation from primary tumour	[50, 3]
Δx	0.03125	discretization step size for \mathcal{G}_Ω	[55]
Δt	10^{-3}	time step size	[55]
$\Delta \eta$	0.0625	mesh size used for \mathcal{G}_M	Estimated
ϵ	0.06967	mollification radius	Estimated

TABLE 1. Summary of parameter values that have used for one population and two sub-population of cancer cells.

REFERENCES

- [1] V. Aaltonen, J. Koivunen, M. Laato and J. Peltonen, Heterogeneity of cellular proliferation within transitional cell carcinoma: Correlation of protein kinase c alpha/betal expression and activity, *Journal of Histochemistry & Cytochemistry* **54** (2006), 795–806.
- [2] J. A. Adam, A simplified mathematical model of tumour growth, *Math. Biosci.* **81** (1986) 229–244.
- [3] V. Andasari, A. Gerisch, G. Lolas, A. South and M. A. J. Chaplain, Mathematical modeling of cancer cell invasion of tissue: biological insight from mathematical analysis and computational simulation, *J. Math. Biol.* **63** (2011), 141–171.
- [4] A. R. A. Anderson, A hybrid mathematical model of solid tumour invasion: the importance of cell adhesion, *Math. Medic. Biol.* **22** (2005), 163–186.
- [5] A. R. A. Anderson, M. A. J. Chaplain, E. L. Newman, R. J. C. Steele and A. M. Thompson, Mathematical modelling of tumour invasion and metastasis, *Journal of Theoretical Medicine* **2** (2000): 490902.
- [6] V. Bitsouni, D. Trucu, M. A. J. Chaplain and R. Eftimie, Aggregation and travelling wave dynamics in a two-population model of cancer cell growth and invasion, *Mathematical Medicine and Biology: A Journal of the IMA* **35** (2018), 541–577.
- [7] H. Byrne, M. Chaplain, G. Pettet and D. L. S. McElwain, A mathematical model of trophoblast invasion, *Appl. Math. Lett.* **14** (2001) 1005–1010.
- [8] H. M. Byrne and M. A. Chaplain, Modelling the role of cell-cell adhesion in the growth and development of carcinoma, *Math. Comput. Model.* **24** (1996), 1–17.
- [9] S. Chakrabarti and F. Michor, Circadian clock effects on cellular proliferation: Insights from theory and experiments, *Current Opinion in Cell Biology* **67** (2020), 17–26.
- [10] M. Chaplain and G. Lolas, Mathematical modelling of cancer cell invasion of tissue: the role of the urokinase plasminogen activation system, *Math. Model. Meth. Appl. Sci.* **15** (2005), 1685–1734.
- [11] M. A. Chaplain, L. Graziano and L. Preziosi, Mathematical modelling of the loss of tissue compression responsiveness and its role in solid tumour development, *Mathematical Medicine and Biology* **23** (2006), 197–229.
- [12] M. E. Davis, Glioblastoma: Overview of disease and treatment, *Clinical journal of oncology nursing* **20** (2016), S2–S8.

- [13] N. E. Deakin and M. A. J. Chaplain, Mathematical modelling of cancer cell invasion: the role of membrane-bound matrix metalloproteinases, *Front. Oncol.* **3** (2013), 1–9.
- [14] H. H. Diebner, T. Zerjatke, M. Griehl and I. Roeder, Metabolism is the tie: The bertalanffy-type cancer growth model as common denominator of various modelling approaches, *Biosystems* **167** (2018), 1–23.
- [15] P. Domschke, D. Trucu, A. Gerisch and M. Chaplain, Mathematical modelling of cancer invasion: Implications of cell adhesion variability for tumour infiltrative growth patterns, *J. Theor. Biol.* **361** (2014), 41–60.
- [16] P. DuChateau and W. Rundell, Unicity in an inverse problem for an unknown reaction term in a reaction-diffusion equation, *Journal of Differential Equations* **59** (1985), 155–164.
- [17] H. W. Engl, K. Kunisch and A. Neubauer, Convergence rates for tikhonov regularization of non-linear ill-posed problems, *Inverse Problems* **5** (1989), 523–540.
- [18] R. A. Gatenby and E. T. Gawlinski, A reaction-diffusion model of cancer invasion, *Cancer Res.* **56** (1996), 5745–5753.
- [19] C. Golias, A. Charalabopoulos and K. Charalabopoulos, Cell proliferation and cell cycle control: a mini review, *International Journal of Clinical Practice* **58** (2004), 1134–1141.
- [20] H. P. Greenspan, On the growth and stability of cell cultures and solid tumours, *J. Theor. Biol.* **56** (1976), 229–242.
- [21] C. Guiot, P. Degiorgis, P. Delsanto, P. Gabriele and T. Diesboeck, Does tumour growth follow a "universal law"?, *Journal of Theoretical Biology* **225** (2003), 147–151.
- [22] D. Hanahan and R. A. Weinberg, The hallmarks of cancer, *Cell* **100** (2000), 57–70.
- [23] D. Hanahan and R. A. Weinberg, The hallmarks of cancer: The next generation, *Cell* **144** (2011), 646–674.
- [24] E. Heitzer and I. Tomlinson, Replicative dna polymerase mutations in cancer, *Current Opinion in Genetics & Development* **24** (2014), 107–113.
- [25] E. Henke, R. Nandigama and S. Ergün, Extracellular matrix in the tumor microenvironment and its impact on cancer therapy, *Frontiers in Molecular Biosciences* **6** (2020), 1–24.
- [26] C. E. Hills, M. Y. G. Younis, J. Bennett, E. Siamantouras, K. K. Liu and P. E. Squires, Calcium-Sensing Receptor Activation Increases Cell-Cell Adhesion and β -Cell Function, *Cell Physiol Biochem* **30** (2012), 575–586.
- [27] A. W. Holle, J. L. Young and J. P. Spatz, In vitro cancer cell-ecm interactions inform in vivo cancer treatment, *Advanced Drug Delivery Reviews* **97** (2016), 270–279.
- [28] T. J. R. Hughes, *The Finite Element Method: Linear Static and Dynamics Finite Element Analysis* (Prentice-Hall, Inc., Englewood Cliffs, New Jersey, 1987).
- [29] B. Kaltenbacher and W. Rundell, On the identification of a nonlinear term in a reaction-diffusion equation, *Inverse Problems* **35** (2019): 115007.
- [30] B. Kaltenbacher and W. Rundell, The inverse problem of reconstructing reaction-diffusion systems, *Inverse Problems* **36** (2020): 065011.
- [31] M. Kühleitner, N. Brunner, W.-G. Nowak, K. Renner-Martin and K. Scheicher, Best fitting tumor growth models of the von bertalanffy-püttertype, *BMC Cancer* **19** (2019): 683.
- [32] A. Laird, Dynamics of tumour growth, *Br. J. Cancer* **18** (1964), 490–502.
- [33] A. López-Carrasco, S. Martín-Vañó, R. Burgos-Panadero, E. Monferrer, A. P. Berbegall, B. Fernández-Blanco, S. Navarro and R. Noguera, Impact of extracellular matrix stiffness on genomic heterogeneity in mycn-amplified neuroblastoma cell line, *Journal of Experimental & Clinical Cancer Research* **39** (2020): 226.
- [34] A. Marusyk and K. Polyak, Tumor heterogeneity: causes and consequences, *Biochimica et biophysica acta* **1805** (2010), 105–117.
- [35] V. A. Morozov, *Methods for solving incorrectly posed problems* (Springer-Verlag New York Inc., 1984), translation ed.: Nashed M. Z. edition.
- [36] M. J. Oudin, O. Jonas, T. Kosciuk, L. C. Broye, B. C. Guido, J. Wyckoff, D. Riquelme, J. M. Lamar, S. B. Asokan, C. Whittaker, D. Ma, R. Langer, M. J. Cima, K. B. Wisinski, R. O. Hynes, D. A. Lauffenburger, P. J. Keely, J. E. Bear and F. B. Gertler, Tumor cell-driven extracellular matrix remodeling drives haptotaxis during metastatic progression, *Cancer Discovery* **6** (2016), 516–531.
- [37] C. D. Paul, P. Mistriotis and K. Konstantopoulos, Cancer cell motility: lessons from migration in confined spaces, *Nature reviews. Cancer* **17** (2017), 131–140.
- [38] L. Peng, D. Trucu, P. Lin, A. Thompson and M. A. Chaplain, A multiscale mathematical model of tumour invasive growth, *Bulletin of mathematical biology* **79** (2017), 389–429.
- [39] A. Perumpanani, D. Simmons, A. Gearing, K. Miller, G. Ward, J. Norbury, M. Schneemann and J. Sherratt, Extracellular matrix-mediated chemotaxis can impede cell migration, *Proceed. Royal Soci. Biol. Sci.* **265** (1998), 2347–2352.
- [40] J. Perumpanani, A.J. Sherratt, J. Norbury and H. Byrne, Biological inferences from a mathematical model for malignant invasion, *Invas. Metast.* **16** (1996), 209–221.

- [41] R. J. Petrie, A. D. Doyle and K. M. Yamada, Random versus directionally persistent cell migration, *Nature Reviews Molecular Cell Biology* **10** (2009), 538–549.
- [42] M. S. Pilant and W. Rundell, An inverse problem for a nonlinear parabolic equation, *Communications in Partial Differential Equations* **11** (1986), 445–457.
- [43] M. S. Pilant and W. Rundell, Iteration schemes for unknown coefficient problems arising in parabolic equations, *Numerical Methods for Partial Differential Equations* **3** (1987), 313–325.
- [44] L. Preziosi and A. Tosin, Multiphase modelling of tumour growth and extracellular matrix interaction: mathematical tools and applications, *J. Math. Biol.* **58** (2009), 625–656.
- [45] P. P. Provenzano, D. R. Inman, K. W. Eliceiri and P. J. Keely, Matrix density-induced mechanoregulation of breast cell phenotype, signaling and gene expression through a fak-erk linkage, *Oncogene* **28** (2009), 4326–4343.
- [46] P. P. Provenzano, D. R. Inman, K. W. Eliceiri, J. G. Knittel, L. Yan, C. T. Rueden, J. G. White and P. J. Keely, Collagen density promotes mammary tumour initiation and progression, *BMC Medicine* **6** (2008): 11.
- [47] K. Psiuk-Maksymowicz, Multiphase modelling of desmoplastic tumour growth, *Journal of Theoretical Biology* **329** (2013), 52–63.
- [48] R. L. Schilling, *Measures, Integrals and Martingales* (Cambridge University Press, 2005).
- [49] A. Sharma, E. Merritt, X. Hu, A. Cruz, C. Jiang, H. Sarkodie, Z. Zhou, J. Malhotra, G. M. Riedlinger and S. De, Non-genetic intra-tumor heterogeneity is a major predictor of phenotypic heterogeneity and ongoing evolutionary dynamics in lung tumors, *Cell Reports* **29** (2019), 2164–2174.
- [50] R. Shuttleworth and D. Trucu, Two-scale moving boundary dynamics of cancer invasion: Heterotypic cell populations’ evolution in heterogeneous ecm, in *Cell Movement Modelling and Applications*, eds. M. Stolarska and N. Tarfulea (Birkhauser, Springer Nature Switzerland AG, 2018), pp. 1–26.
- [51] R. Shuttleworth and D. Trucu, Multiscale modelling of fibres dynamics and cell adhesion within moving boundary cancer invasion, *Bulletin of mathematical biology* **81** (2019), 2176–2219.
- [52] H. Takahashi, M. Asaoka, L. Yan, O. M. Rashid, M. Oshi, T. Ishikawa, M. Nagahashi and K. Takabe, Biologically aggressive phenotype and anti-cancer immunity counterbalance in breast cancer with high mutation rate, *Scientific Reports* **10** (2020): 1852.
- [53] K. M. C. Tjorve and E. Tjorve, The use of Gompertz models in growth analyses, and new Gompertz-model approach: An addition to the Unified-Richards family, *PLOS ONE* **12** (2017), 1–17.
- [54] M. Tomkova, J. Tomek, S. Kiaucionis and B. Schuster-Böckler, Mutational signature distribution varies with dna replication timing and strand asymmetry, *Genome Biology* **19** (2018): 129.
- [55] D. Trucu, P. Lin, M. A. J. Chaplain and Y. Wang, A multiscale moving boundary model arising in cancer invasion, *Multiscale Model. Simul.* **11** (2013), 309–335.
- [56] S. Vincenzi, D. Jesensek and A. J. Crivelli, Biological and statistical interpretation of size-at-age, mixed-effects models of growth, *Royal Society Open Science* **7** (2020), 192146.
- [57] S. Webb, J. Sherratt and R. Fish, Alterations in proteolytic activity at low ph and its association with invasion: a theoretical model, *Clin. Experim. Metast.* **17** (1999), 397–407.
- [58] M. C. Weiger, V. Vedham, C. H. Stuelten, K. Shou, M. Herrera, M. Sato, W. Losert and C. A. Parent, Real-time motion analysis reveals cell directionality as an indicator of breast cancer progression, *PLOS ONE* **8** (2013), 1–12.
- [59] R. A. Weinberg, *The Biology of Cancer* (Garland Science, New York, 2006).
- [60] P.-H. Wu, A. Giri, S. X. Sun and D. Wirtz, Three-dimensional cell migration does not follow a random walk, *Proceedings of the National Academy of Sciences* **111** (2014), 3949–3954.
- [61] K. Yosida, *Functional Analysis* (Springer-Verlag, 1980), 6th edition.
- [62] J. Zhu and C. B. Thompson, Metabolic regulation of cell growth and proliferation, *Nature Reviews Molecular Cell Biology* **20** (2019), 436–450.

DIVISION OF MATHEMATICS, UNIVERSITY OF DUNDEE, DUNDEE DD1 4HN, UNITED KINGDOM
 E-mail address: m.s.z.alwuthaynani@dundee.ac.uk

CORRESPONDING AUTHOR, DIVISION OF MATHEMATICS, UNIVERSITY OF DUNDEE, DUNDEE DD1 4HN, UNITED KINGDOM
 E-mail address: trucu@maths.dundee.ac.uk